Loss of function mutations in KIF14 cause severe microcephaly and kidney development defects in humans and zebrafish

Madeline Louise Reilly, Marijn F Stokman, Virginie Magry, Cécile Jeanpierre, Marine Alves, Mohammadjavad Paydar, Jacqueline Hellinga, Marion Delous, Daniel Pouly, Marion Failler, et al.

Loss of function mutations in *KIF14* cause severe microcephaly and kidney development defects in humans and zebrafish.

Madeline Louise Reilly[1,2] , Marijn F. Stokman[3], Virginie Magry[1], Cecile Jeanpierre[1], Marine Alves[1], Mohammadjavad Paydar[4], Jacqueline Hellinga[5], Marion Delous[1], Daniel Pouly[1], Marion Failler[1], Jelena Martinovic[6,7], Laurence Loeuillet[8], Brigitte Leroy[9], Julia Tantau[9], Joelle Roume[10], Cheryl Gregory Evans[11], Xianghong Shan[11], Isabel Filges[12,13,14,], John S. Allingham[5], Benjamin H. Kwok[4], Sophie Saunier[1], Rachel H. Giles[15] and Alexandre Benmerah[1,*]

[1] Laboratory of Hereditary Kidney Diseases, INSERM UMR 1163, Paris University, Imagine Institute, 75015 Paris, France.

[2]Paris Diderot University, 75013 Paris, France.

[3]Department of Genetics, University Medical Center Utrecht, Utrecht University, Utrecht, Netherlands.

[4]Institute for Research in Immunology and Cancer (IRIC), Département de médecine, Université de Montréal, P.O. Box 6128, Station Centre-Ville, Montréal, QC H3C 3J7, Canada.

[5]Department of Biomedical and Molecular Sciences, Queen's University, Kingston, ON K7L 3N6, Canada.

[6]Unit of Fetal Pathology, Antoine Béclère Hospital, AP-HP, 92140 Clamart, France.

[7]INSERM U-788, Génétique/ Neurogénétique, 94270 Kremlin-Bicêtre, France.

[8]Service d'Histologie-Embryologie-Cytogénétique, Hôpital Necker-Enfants Malades, AP-HP, 75015 Paris, France.

[9]Service d'Anatomie et de Cytologie Pathologiques, CHI Poissy, 78100 Saint Germain en Laye, France.

[10]Service de Génétique, CHI Poissy, 78100 Saint Germain en Laye, France.

[11]Department of Ophtalmology, University of British Columbia, Vancouver, Canada.

[12]Medical Genetics, Institute of Medical Genetics and Pathology, University Hospital and University of Basel, Basel, Switzerland.

[13]Department of Clinical Research, University Hospital and University of Basel, Basel, Switzerland.

[14]Department of Genetics, University of British Columbia, Vancouver, Canada

[15]Department of Nephrology and Hypertension, University Medical Center Utrecht, Utrecht University, Utrecht, Netherlands.

* To whom correspondence should be addressed:

Alexandre Benmerah, Laboratory of Inherited Kidney Diseases, Institut Imagine, 24 boulevard du Montparnasse, 75015 PARIS, France. tel: +33 1 42 75 43 44, fax: +33 1 42 75 42 25, email: alexandre.benmerah@inserm.fr

Abstract:

Mutations in *KIF14* have previously been associated with either severe, isolated or syndromic microcephaly with renal hypodysplasia (RHD). Syndromic microcephaly-RHD was strongly reminiscent of clinical ciliopathies, relating to defects of the primary cilium, a signalling organelle present on the surface of many quiescent cells. *KIF14* encodes a mitotic kinesin which plays a key role at the midbody during cytokinesis and has not previously been shown to be involved in cilia-related functions. Here, we analysed four families with foetuses presenting with the syndromic form and harbouring biallelic variants in *KIF14*. Our functional analyses show that the identified variants severely impact the activity of KIF14 and likely correspond to loss-of-function mutations. Analysis in human foetal tissues further revealed the accumulation of KIF14-positive midbody remnants in the lumen of ureteric bud tips indicating a shared function of KIF14 during brain and kidney development. Subsequently, analysis of a *kif14* mutant zebrafish line showed a conserved role for this mitotic kinesin. Interestingly, ciliopathy-associated phenotypes were also present in mutant embryos, supporting a potential direct or indirect role for KIF14 at cilia. However, our *in vitro* and *in vivo* analyses did not provide evidence of a direct role for KIF14 in ciliogenesis and suggested that loss of *kif14* causes ciliopathy-like phenotypes through an accumulation of mitotic cells in ciliated tissues. Altogether, our results demonstrate that *KIF14* mutations result in a severe syndrome associating microcephaly and RHD through its conserved function in cytokinesis during kidney and brain development.

Introduction:

Congenital Anomalies of the Kidney and Urinary Tract (CAKUT) comprise a broad spectrum of renal and urinary tract malformations of varying severity. Kidney defects can range from unilateral or bilateral renal agenesis to renal hypodysplasia (RHD), or include multicystic kidney dysplasia (1). The latter can also be part of the phenotypic spectrum of foetal forms of ciliopathies (Meckel-Gruber syndrome, MKS), linked to mutations in genes encoding key components of primary cilia (PC) (2). RHD results from defects during differentiation of the metanephros, initiated by a reciprocal induction between the ureteric bud (UB) and the metanephric mesenchyme. The UB invades the metanephric mesenchyme and undergoes several rounds of branching, expanding through the proliferation of UB tip epithelial cells to form the collecting ducts. Inductive signals from the UB drive the condensation of metanephric mesenchyme cells at the tips of the UB branches to form the cap mesenchyme. These cells undergo a mesenchyme-to-epithelial transition to form the renal vesicle, which will differentiate into several intermediate structures (comma body, then S-shaped body) to finally form the nephron, the functional unit of the kidney. The proximal region of the S-shaped body will differentiate to give rise to the blood-filtering glomerulus, while the distal region will connect to the collecting ducts. Nephrogenesis takes place in the cortex of the developing kidneys and ends before birth (35-36 weeks) in humans (3, 4).

The mouse has been a widely used model to decipher the mechanisms controlling nephrogenesis, as many of the processes involved in metanephric kidney development are well conserved (3, 4). However, zebrafish have recently become a powerful alternative model for both kidney development and disease modelling (5, 6). The pronephros of zebrafish larvae is functional and consists of two nephrons with a fused glomerulus. Early development of the zebrafish pronephros requires the condensation of progenitors into two epithelial tubes, which retain a pattern of segmentation similar to that of mammalian nephrons. A functional kidney is formed by 48 hours post-fertilisation (hpf) through the frontward migration of cells towards the glomerulus, along with spatially and temporally controlled waves of mitosis (5, 6).

To date, mutations resulting in RHD in humans have been identified in more than 50 genes with a role in kidney development, revealing a great genetic heterogeneity (1, 7). Most of these genes encode transcription factors (PAX2, SIX1, EYA1, HNF1B) and actors in key signalling pathways (RET-GDNF, FGF, NOTCH). Few of these genes were associated with bilateral renal agenesis (8–10). Interestingly, biallelic LOF mutations in *KIF14*, encoding a mitotic kinesin required for cell abscission, were recently reported in foetuses presenting with bilateral renal agenesis or RHD, associated with complex brain malformations including very severe microcephaly (11, 12).

Microcephaly is a condition in which foetuses or infants present with a very small head and brain, and is part of a family of highly heterogeneous disorders grouped under the term of malformations of cortical development (MCD). The initial phase of brain development depends on an intense phase of progenitor proliferation within the ventricular zone. Symmetrical mitosis of these progenitor cells occurs at the apical face of the neuroepithelium, lining the lumen of the neural tube. Following this initial amplification phase, cells begin to divide asymmetrically and waves of committed, post-mitotic cells undergo an active phase of migration (13). Defects in any of these complex events lead to MCD or microcephaly. Microcephaly, like CAKUT, is genetically heterogeneous, with mutations identified in genes regulating signalling pathways, microtubule dynamics and mitotic spindle orientation, including several kinesin family members (14).

Kinesins are molecular motors known to bind their respective cargos through their C-terminal domain and microtubules through their motor domain. Following these interactions, the kinesin then moves along microtubules, usually in a plus-end directed manner, through the hydrolysis of ATP (15). KIF14 is a member of the Kinesin 3 family, which is highly conserved during evolution and possesses a slow processive activity (16). It was identified as a key actor of cytokinesis (17, 18), the last step of mitosis leading to separation of the two daughter cells (19), through its interaction with PRC1 and citron kinase (CIT) (18, 20). KIF14 accumulates at the spindle midzone and the midbody, where it is recruited by CIT (18). KIF14 also acts reciprocally to ensure the correct distribution of CIT within this latter structure (20, 21). Although initially considered an artefact, the formation of the midbody, or Flemming

body, is now known to be crucial for the completion of mitosis (22). Proteins involved in cleavage furrow ingression accumulate between the two parts of the intercellular bridge and recruit components of the ESCRT machinery to ensure scission of the plasma membrane at one or both sides of this central structure, which is then either inherited by one daughter cell or "secreted" into the extracellular milieu (22). Unsurprisingly therefore, depletion of KIF14 in HeLa cells leads to cytokinesis defects and binucleated cells (17, 18). Besides its role during cytokinesis, KIF14 regulates migration in cancer cells via C-terminal interactions with RADIL (23).

In vivo, loss of KIF14 in *Drosophila* leads to cytokinesis and developmental defects (24–27) and in mice to microcephaly and growth retardation (28). In humans, in addition to the syndromic cases associating severe microcephaly and RHD (11, 12), mutations in *KIF14* were recently identified in isolated, mild- to severe- microcephaly (29, 30), with a phenotypic spectrum similar to that observed in cases of *CIT* mutations (31–34). In these reports, microcephaly was not associated with major kidney malformations in any of the individuals harbouring mutations in either *KIF14* or *CIT*. In addition, as the clinical features of syndromic cases showed a partial overlap with the phenotypic spectrum of MKS (intrauterine growth restriction, cystic kidneys and brain developmental defects, including cerebellar hypoplasia and vermis agenesis), *KIF14* was subsequently termed *MKS12* (OMIM 616258). All proteins encoded by MKS genes identified thus far are present at the primary cilium and so KIF14 was proposed to have a ciliary function.

The main objective of this study was to further characterise the phenotypic spectrum associated with mutations in *KIF14* and to better understand its role during kidney development. We describe novel biallelic *KIF14* mutations in foetuses presenting with RHD and microcephaly. We analyse the functional effects of the mutations identified in four families and their consequences on cytokinesis and the potential role of KIF14 in ciliogenesis. We also use the zebrafish model to investigate the consequences of the loss of KIF14 *in vivo*, demonstrating a conserved function during both kidney and brain development. Finally, we provide direct evidence for similarities and distinctions between mitotic events occurring during proliferation in both brain and kidney development.

Results:

Mutations in *KIF14* cause a lethal, highly penetrant syndromic CAKUT with microcephaly.

In addition to the initial family that we described several years ago (11), we identified a further four families (Families 1 to 4) with foetuses presenting with highly reminiscent phenotypes, microcephaly and cystic RHD or bilateral renal agenesis (Fig. 1A and B; Supplementary Material, Table S1), linked to biallelic mutations in *KIF14*. Mutations identified in family 1 and 2 have been reported recently (12), while those in family 3 and 4 have never been described.

Whole- or targeted-exome sequencing approaches enabled the identification of biallelic pathogenic variants in *KIF14* in all these families (Fig. 1A and B; Supplementary Material, Table S1). The affected foetus in family 1 harboured a homozygous out-of-frame deletion of exons 23, 24 and 25 (c.[3567-?_4072+?del]) leading to a frameshift (p.Arg1189Argfs*9). Compound heterozygous variations associating a predicted damaging missense variation in the motor domain (c.1090C>T [p.Arg364Cys] or c.1367C>T [p.Thr456Met]) with a nonsense mutation predicted to lead to a loss of the C-terminal region of the protein (c.3910C>T [p.Gln1304*] or c.4138C>T [p.Gln1380*]) were identified in families 2 and 3 respectively. Finally, the affected foetus in family 4 harboured a homozygous nonsense mutation predicted to lead to an early truncation in the motor domain (c.1792C>T [p.Arg598*]). All variations were absent from in-house and public databases (gnomAD) and missense variants were predicted damaging by Polyphen and Sift (0.787/0.01 for Thr456Met; (12)). Segregation of the identified mutations with the developmental defects was confirmed for all the families by Sanger sequencing. The parents were heterozygous, while affected foetuses, where DNA was available, harboured the corresponding biallelic variations in *KIF14* (Supplementary Material, Table S1 and Fig. S1A-C; (12)).

Despite the heterogeneity of the variations identified in these families, all the affected foetuses presented with strikingly similar severe brain and kidney phenotypes (Supplementary Material, Table S1). All affected foetuses presented with microcephaly with a flattened forehead (Fig. 1C-E; Supplementary Material, Fig. S1D). Autopsy revealed a strong delay in the development of the telencephalon (white arrows) leading to agenesis of the occipital lobes and corpus callosum. Additionally, all affected foetuses

presented hypoplasia of the cerebellum (white arrowheads) with foliation delay (Fig. 1C-E, Supplementary Material, Fig. S1; Table S1). The kidney phenotype was equally severe, with either bilateral renal agenesis (3/11 cases), severe non cystic (2/11) or cystic RHD (6/11; Fig. 1C and E, black arrows). Histochemistry of the cystic kidneys revealed, in addition to large cortical cysts, a lack of nephrogenic zone and absence of corticomedullary differentiation (Fig. 1C-E). Few glomeruli could be observed (black arrowheads), some were cystic (in families 1, 2 and 4; black asterisks), and tubules were rare (Fig. 1C and E; Supplementary Material, Figs. S1 and S2) and surrounded by undifferentiated mesenchymal tissue. Immunohistochemistry confirmed the lack of nephrogenic zone (PAX2/SIX2 stainings) in foetuses from families 1 and 3 and the presence of few remaining glomeruli in foetus 1 from family 1 (Supplementary Material, Fig. S2A and B).

Altogether these results clearly demonstrate that biallelic mutations in *KIF14* lead to a syndrome characterised by severe developmental defects in both brain and kidney leading to arhinencephaly/atelencephaly and RHD.

Identified variations have a strong impact on KIF14 activity.

Kinesins bind microtubules through their motor domain, which in many cases is negatively regulated through intramolecular interactions with the C-terminal cargo-binding domain (15). In the case of KIF14, this negative regulation of the motor domain is released upon interaction with CIT, which binds to the C-terminal region of KIF14 (aa 901-1233) through its N-terminal coiled-coil domain (CCf domain; (21)). As the mutations identified affect the two key domains of KIF14, we predicted that they would have dramatic functional effects.

We first tested the consequences of the missense and truncation mutations on the steady state localisation of KIF14. Depending on the activation state, KIF14 could either be found diffusely distributed in the cytoplasm when expressed in non-mitotic HeLa cells (17, 18, 21) or on microtubules upon activation (21). Accordingly, a GFP-fusion encoding wild-type (WT) KIF14 revealed a diffuse cytoplasmic localisation (Fig. 2A) which was unaffected by the missense variations, T456M and R364C

(Fig. 2B and C). In contrast, the C-terminal truncations (Q1380*, Q1304* and R1189*) all affected KIF14 localisation and impacted upon cell morphology (Fig. 2D-F). The Q1380* mutant strongly accumulated at the tips of transfected cells, which became highly elongated, and where it colocalised with acetylated α-tubulin (AcTub; Fig. 2D), a marker of stabilised microtubules. Both Q1304* (Fig. 2E) and R1189* (Fig. 2F) were present along stable microtubules, colocalising with AcTub, and could occasionally be observed accumulated at the extremities of microtubules at the cell periphery. These observations suggest that the C-terminal truncations lead to constitutively active forms of KIF14 which are capable of binding microtubules. The procession of these active forms, particularly Q1380*, towards the plus-ends of microtubules appears to cause a stabilisation of microtubules, resulting in distension of the cell into protrusions, as was previously characterised for other Kinesin family members (15).

As CIT is one of the main partners of KIF14 and regulates its activity (21), we next investigated the impact of the identified mutations on this interaction. We performed co-immunoprecipitation assays from lysates of HEK293 renal cells co-expressing WT or variant forms of KIF14 and the KIF14-binding domain of CIT (CCf; Fig. 2G). As expected, the CIT CCf domain was efficiently co-immunoprecipitated with WT KIF14 but not with the N-terminal PRC1 binding domain (1-356). This interaction was unaffected by the missense mutations in the motor domain (R364C, T456M) and by the two more C-terminal truncation mutations (Q1304*, Q1380*), which are localised after the previously mapped CIT binding site (aa 901-1233; Fig. 2H). Surprisingly, the most N-terminal truncation variation, R1189*, also retained the interaction (Fig. 2G) despite being expected to result in the partial truncation of the CIT binding domain (Fig. 2H). This result indicates that the CIT interaction domain of KIF14 in fact lies between amino acids 901 and 1189 (Fig. 2H).

As the nonsense mutation in the motor domain (family 4) was very similar to that previously described (11) and those of the mouse model (28), their negative impact was not investigated here. In contrast, the functional consequence of the missense variations identified in families 2 and 3 remained to be demonstrated. Site-directed mutagenesis has identified amino acids crucial to the activity of the motor domain, usually relating to ATP-binding and hydrolysis. Arg364 (Fig. 3A), which is replaced by Cys in

family 2, is analogous to Arg14 in conventional Kinesin, which, when mutated, was shown to result in a severe reduction of MT-gliding velocity (35). The p.Arg364Cys variation is therefore expected to result in loss-of-function of the KIF14 motor domain. Based on the resolved structure of the murine Kif14 motor domain (16), the Thr456 residue (Thr491 in mouse), replaced by Met in family 3, is part of the ATP-binding pocket of KIF14 where it faces Arg364 (Fig. 3A). This variation was therefore also expected to severely impact the function of the motor domain, which was investigated using a MT sedimentation assay. As previously demonstrated for the murine Kif14 motor domain (16), the human KIF14 motor domain efficiently co-pelleted with microtubules (Fig. 3B). The introduction of the p.Thr456Met variation (T456M) severely impaired MT binding, and the mutant motor domain remained within the supernatant (Fig. 3B). In addition, measurement of the ATPase activity of the motor domains revealed that ATP hydrolysis remained unchanged after the addition of microtubules to the T456M mutant (Fig. 3C). Similar results were obtained with the murine motor domain, where the equivalent human variant was introduced and compared to the WT (T491M; Supplementary Material, Fig. S3).

Previous work established that the CIT interaction activates KIF14 and allows its binding to microtubules (21). In contrast to WT KIF14 (Fig. 3D, arrows), R364C and T456M variants did not colocalise with α-tubulin when co-expressed with the CCf domain of CIT (Fig. 3E and F). As the missense variants retain the ability to bind CIT (Fig. 2), these data show that both variations severely impair the ability of the motor domain to bind microtubules, thus rendering these variant kinesins non-functional.

In conclusion, all identified variants could thus be considered as strongly damaging mutations.

Loss of *KIF14* result in defects in cytokinesis *in vitro* and *in vivo*

Previous *in vitro* work has focused on the impact of a transient loss of KIF14 in HeLa cells (17, 18). In order to better characterise the effect *KIF14*-loss in stable conditions in kidney cells, we performed a knockout of the gene in murine inner medullary collecting duct cells (mIMCD3), a widely used model of kidney epithelial cells. We used CRISPR/Cas9 (nickase) with guides targeting exon 5 encoding part of the

motor domain (Supplementary Material, Fig. S4A). Clones were isolated and sequenced to identify homozygous mutational events. Two clones (KO1 and KO2), both with partial deletions of the 3' region of exon 5 and 5' region of intron 5-6 (Supplementary Material, Fig. S4B), were selected for further analysis. Sequencing of RT-PCR products revealed that the exon/intron deletions resulted in exon skipping in both clones, which could lead to an in-frame deletion in KO1 (exon5+6) and/or to a frameshift and early stop codon in exon 6 in both KO1 and KO2 (Supplementary Material, Fig. S4C-E). These events likely result in non-functional proteins since they generate short truncated forms and/or proteins lacking a stretch of 28 aa within the motor domain. Two clones in which no mutational events in *Kif14* could be identified (WT1 and WT2) and which expressed similar levels of Kif14 to the parental cell line (Supplementary Material, Fig. S4F) were maintained as controls.

While Kif14 (green) was detected at the midbody in parental IMCD3 cells (not shown) and control WT clones, it was absent from the intercellular bridges (AcTub staining, red) of KO clones (Fig. 4A), which were elongated compared to those of controls (Fig. 4B). In addition, CIT localisation at the midbody was affected in KO clones, showing either a diffuse distribution along bridges or being present as two rings instead of a unique one (Fig. 4C and D), as previously described (Watanabe 2013). Consequently, the loss of Kif14 in KO clones led to an increase in the proportion of binucleated cells (Fig. 4E and F). Interestingly, similar defects were observed in fibroblasts obtained from the affected foetus 21 from family 4 with longer intercellular bridges (Fig. 4G and H) and increased proportion of binucleated cells compared to control (Fig. 4I and J).

Human kidney development is severely impaired in cases where KIF14 function is lost, with affected foetuses presenting with either bilateral renal agenesis or cystic RHD (Fig. 1; Supplementary Material, Fig. S1). To explore the role of this mitotic kinesin in development, we analysed the protein localisation in tissue sections from normal human foetal kidneys. Sections were stained for both KIF14 (green) and PAX2 (red), a marker of epithelial and mesenchymal components of the developing kidney (3, 4). Strikingly, the lumen of some PAX2-positive epithelial structures were filled with KIF14-positive dots which, when observed at a higher magnification, appeared as rings (Fig. 5A), indicative of the presence of

KIF14-positive midbodies in UB tips lumen. In agreement with this observation, CIT (green) showed a similar ring-shaped pattern in the lumen of PAX2-positive structures surrounded by SIX2-positive cells (cyan; Fig. 5B), a marker of the cap mesenchyme. Finally, we observed a colocalisation of both KIF14 (green) and CIT (cyan) in ring-shaped structures within clearly identifiable PAX2-positive UB branch tips (red; Fig. 5C).

These results were suggestive of a luminal accumulation of midbodies or midbody remnants following mitosis. Interestingly, mitosis of the epithelial cells of the UB tips was shown to occur in the lumen, with the daughter cell bodies subsequently reinserting into the epithelium ((36), see discussion). In this context, it was expected that the cytokinesis failure induced upon loss of KIF14 would generate binucleated cells, which should then be found in the lumen or epithelium layer. Careful analysis of kidney sections from affected foetuses revealed the presence of binucleated cells protruding from the surface of the epithelium along the lumen of large cysts (Fig. 5D and E) or inside the lumen of smaller cystic structures (Fig. 5F and G). As expected, numerous binucleated cells were also found in the cortex of the older affected foetus (51.5% (102/198) binucleated pyramidal cells vs 0.5% (1/200) in control; Fig. 5H-K). Binucleated Purkinje cells could be found in the cerebellum of the affected foetus (Fig. 5L-O), they were, however, rare compared to cells in the cortex, reflecting the less pronounced defect in cerebellar development in the affected foetus (Supplementary Material, Table S1).

In conclusion, KIF14 plays a crucial function in cytokinesis during kidney and brain development.

Loss of *kif14* in zebrafish causes microcephaly and ciliopathy-related phenotypes.

A previous *in vivo* study in mice demonstrated that the loss of Kif14 resulted in microcephaly and growth restriction but failed to replicate the kidney phenotype observed in humans (28). We therefore chose to use the zebrafish as an alternative *in vivo* model in order to explore a potential conserved kidney specific role for KIF14.

A mutant line was acquired from the Zebrafish Mutation Project (Sanger Institute; sa24165 (37)), in which a single nucleotide substitution resulted in a nonsense mutation and an early truncation after the

motor domain (c.1870C>T[p.Gln624*]; Fig. 6A), a mutation similar to those identified in affected foetuses. The presence of the mutation was confirmed by Sanger sequencing (Fig. 6B). Macroscopically visible phenotypes (see below) were observed in ¼ of the embryos from crosses of heterozygous (Htz) individuals and Sanger sequencing confirmed that the affected larvae were homozygous for the mutation, hereafter *kif14*$^{-/-}$. These phenotypes were 100% penetrant in *kif14*$^{-/-}$ homozygous embryos, while heterozygous embryos were indistinguishable from WT siblings. *kif14*$^{-/-}$ embryos were not viable and died by 5 days post fertilisation. By 48 hours post fertilisation (hpf), they demonstrated microcephaly, eye defects, body curvature, which could be dorsal, ventral or lateral, and cardiac oedema (Fig. 6C). Similar phenotypes were also observed in *kif14* morphants (Supplementary Material, Fig. S5).

Data from zebrafish models of brain development have demonstrated that morphogenesis occurs first through the establishment of the forebrain, midbrain and hindbrain ventricles between 17 and 21 hpf, followed by expansion of the ventricles between 21 and 36 hpf (38). Microcephaly in mutant *kif14*$^{-/-}$ embryos was evident around 22 hpf, with an absence of clear ventricular definition on both lateral and dorsal views (Fig. 6D and E). As shown in many microcephaly models (39), immunofluorescence staining for phospho-histone H3 (PH3), a marker of cells in G2/M, revealed a significant increase in the number of mitotic cells in *kif14*$^{-/-}$ embryos, notably in the brain and along the spine, but also in peripheral tissues (Fig. 6F). Similarly, *kif14*$^{-/-}$ mutant embryos also present microphthalmia (Fig. 6D, G and H), with a delay of optic fissure closure and occasional coloboma (Fig. 6G, blue arrows). In addition, the *kif14*$^{-/-}$ embryos presented with cardiac oedema (Fig. 6C and D, lower row), often an indication of pronephric cysts (5, 40). In order to examine the potential kidney defects, we used the *Tg(wt1b:GFP)* transgenic line expressing GFP under the control of the *wt1b* promoter (41). GFP expression in the proximal pronephros allowed us to confirm the presence of glomerular cysts in *73%* of *kif14*$^{-/-}$ mutant embryos at 48hpf (n=47, 4 separate clutches; Fig. 6I). Altogether, these data show that the loss of *kif14* in zebrafish recapitulates both the brain and kidney developmental phenotypes observed in the affected foetuses.

Loss of *kif14* causes ciliopathy-related phenotypes possibly due to an accumulation of mitotic cells in ciliated tissues.

Pronephric cysts and body curvature are among the phenotypes widely seen in zebrafish models of known ciliopathy genes (5, 40). Otolith defects are also commonly observed in ciliopathy models. Otoliths are structures present within the lumen of the otic vesicle and composed of biominerals. Their formation at the tips of tether cilia of sensory neurons has been shown to rely, at least partially, on the presence of motile cilia at the luminal surface of the neuroepithelium (42).

We observed a variety of otolith defects at 72hpf in *kif14*$^{-/-}$ embryos (Fig. 7A and B). Most otoliths were smaller, with many incorrectly positioned within the vesicle (misplaced). Occasionally, otoliths were fused, or present as a single structure, whilst extranumerary (extra) otoliths were rare. To directly explore whether these defects were related to cilia dysfunction within the otic vesicle, we used a transgenic (Tg) line in which the ciliary membrane marker Arl13b is fused to GFP and ubiquitously expressed (Tg(*act2b:Arl13b-GFP*); (43)). Confocal imaging of WT larvae (24hpf) showed that the Arl13b fusion stained cilia present all cilia on neuroepithelial cells lining the lumen of the otic vesicle. Analysis in mutant embryos revealed that the number of cilia per otic vesicle was severely decreased compared to WT siblings (Fig. 7C and D). Taken together with the other phenotypes, these observations indicated that the loss of *kif14* was impacting ciliogenesis.

To elucidate whether KIF14 plays a direct role in ciliogenesis, we initially tested two widely used *in vitro* models, IMCD3 and RPE1 cells, in which primary cilia formation can be easily monitored and are therefore the two most widely used models to study ciliogenesis. Loss of *KIF14* by either transient siRNA-mediated knockdown in RPE1 (Supplementary Material, Fig. S6A-D) or stable KO in IMCD3 (Supplementary Material, Fig. S6E-G) did not have a significant effect on the percentage of ciliated cells and cilia length compared to controls. We subsequently investigated the impact of the loss of *kif14* on cilia in the cloaca region of zebrafish embryos, where cilia are affected in many ciliopathy models (44, 45). Ciliogenesis in this distal part of the pronephros was not affected in *kif14*$^{-/-}$ embryos (Supplementary Material, Fig. S6H-J) supporting the conclusion that KIF14 does not play a general role in ciliogenesis.

Cilia are present in quiescent cells and resorbed when cells enter in mitosis, mitotic cells are therefore not ciliated (ref (46) and Supplementary Material, Fig. S7A). Interestingly, analysis of *kif14*$^{-/-}$ zebrafish revealed a drastic increase in the number of mitotic PH3+ cells (Fig. 6F). In addition, AcTub stainings revealed the presence of numerous cells with mitotic spindle and condensed chromosomes around the distal end of the pronephros (Supplementary Material, Fig. S6H, arrows). These results then suggested that the ciliogenesis defects observed in the otic vesicle of *kif14*$^{-/-}$ embryos could be linked to the accumulation of mitotic, non-ciliated cells. To test this hypothesis, we stained for PH3 in the *Tg(cldnB:lynGFP)* line in which neuroepithelial cells lining the otic vesicle express GFP (47). Confocal imaging of 24 hpf embryos revealed a drastic increase in the number of mitotic cells in the otic vesicle in *kif14*$^{-/-}$ mutant embryos (Fig. 7E and F), mirroring ciliogenesis defects in this organ (Fig. 7C and D) and correlating with the accumulation of mitotic non-ciliated cells (Supplementary Material Fig.7B). We then similarly analysed mitosis in the pronephros. As expected (48), very few PH3+ cells could be observed in proximal (*wt1b:GFP*; Supplementary Material, Fig. S8A and B) and distal (*cldnB:GFP*; Supplementary Material, Fig. S8C and D) tubules at 48hpf, in WT/Htz embryos. However, the number of mitotic cells was drastically increased in *kif14*$^{-/-}$ embryos in both regions.

Taken together, these data show that the loss of *kif14* in zebrafish causes ciliopathy-like phenotypes, including in the otic vesicle and pronephros, which are likely linked to an accumulation of mitotic, and therefore non-ciliated cells in those tissues. In addition, this accumulation of mitotic cells indicates that *kif14* may play an additional role during the early stages of mitosis in zebrafish.

Discussion:

The present study, in accordance with our previous one, describes a novel syndrome linked to mutations in *KIF14* and associated with severe developmental defects of both the brain (microcephaly/atelencephaly) and kidney (RHD). Here, we provide functional evidence that mutations in the syndromic form cause a loss-of-function of *KIF14*. In addition, we used the zebrafish model to provide strong evidence that kif14 plays a crucial and conserved role during both brain and kidney development.

Two other groups recently identified mutations in *KIF14* in eight families with individuals presenting mild to severe microcephaly without major renal malformation (except one case out of 18; Supplementary Material, Fig. S9). Comparing the effect of these mutations provides some clues to explain the broad phenotypic spectrum associated with KIF14 mutations. Among the syndromic forms, two families harbour mutations leading to an early stop codon within the motor domain. These mutations are likely to correspond to a knock-out of KIF14 as even if alternative splicing were induced, any exon skipping in this region would lead to disruption of the motor domain. In addition, our functional studies clearly show that the mutations identified in the 3 other syndromic cases are also LOF mutations leading either to variant proteins unable to bind microtubules (motor domain), or to active non-functional forms which lack the C-terminal domain, encoding at least a regulatory domain (this study) and the Radil binding site (23). Interestingly, our results also show that a truncation mutation of *kif14* in the zebrafish, similar to those identified in humans, mimics the human syndromic form, further indicating that these truncation mutations result in non-functional proteins.

On the contrary, analysis of the mutations described in the 8 families with isolated microcephaly (29, 30) indicates that they are likely to be less severe. Three missense mutations and a single amino acid deletion are located in the FHA domain, a domain which has regulatory functions in some kinesin family members (15) but whose function has not yet been characterised in KIF14. One missense mutation leads to a deletion of a smaller part of the C-terminal tail and missense or silent mutations affect splice sites, leading to the co-expression of C-terminally truncated proteins and missense variant or WT proteins, respectively. Interestingly, one mutation was also found in the motor domain (p.Gly459Arg); however,

unlike both the Arg364 and Thr456 residues, the Gly459 residue is not present within the nucleotide binding pocket. It is likely, therefore, that the functional consequences of the p.Gly459Arg mutation would be far less severe than the p.Arg364Cys and p.Thr456Met mutations described here. Finally, the c.246delT/p.Asn83Ilefs*3 homozygous mutation described in a family with individuals presenting with microcephaly without kidney defects, would be expected to be even more severe than the ones in our syndromic families. Interestingly, it is in the same region as the c.263T>A/p.Leu88* mutation which was shown to activate a cryptic splice site and to lead to an in-frame deletion within exon 2, resulting in a deletion of 124 aa (p.G58_L181del) within the PRC1-binding domain. The potential consequences on splicing of the c.246del/p.Asn83Ilefs* mutation remain to be tested in order to conclude on the lack of genotype/phenotype correlation for this specific case.

Therefore, we can conclude that LOF mutations in KIF14 lead to syndromic forms associating microcephaly and brain malformations with RHD, whereas hypomorphic mutations cause mild to severe microcephaly with no developmental kidney defects. The observation of small echogenic kidneys in one affected individual (out of 18), however, indicates the potential for kidney manifestations in individuals harbouring hypomorphic *KIF14* mutations.

Altogether, these results suggest that KIF14 likely has an important and similar function during the early steps of both kidney and brain development. There are very few reports of monogenic mutations identified in syndromes associating MCD or microcephaly with kidney phenotypes (Galloway-Mowat (49) and DREAM-PL (34) syndromes). However, the kidney phenotypes in these syndromes, including glomerulopathy or occasional unilateral agenesis, are much less severe than those observed in the case of *KIF14* mutations. It is worth noting that associations of renal agenesis/RHD and MCD/microcephaly, reminiscent of those observed in individuals with *KIF14* mutations, were described in cases with copy number variations of varying sizes and at various loci, suggesting the involvement of one or several genes which were not characterised further (50). Finally, while mutations in genes involved in microtubule dynamics, mitosis and/or orientation of the mitotic spindle represent a major cause of microcephaly (14),

it is not the case for renal agenesis and RHD with none of the mutations identified thus far affecting genes from these functional families (see (12, 50) for a recent list of CAKUT genes).

Ciliary defects were a plausible pathophysiological explanation for the two distinct phenotypes in foetuses harbouring LOF *KIF14* mutations, as suggested earlier (11). Central nervous system manifestations are also observed in patients presenting with renal ciliopathies, such as cerebellar hypoplasia or agenesis of the corpus callosum, two defects that are present in all the affected foetuses. A plethora of brain developmental disorders are recognised clinical signs in many ciliopathy phenotypes (2), but the direct role of mutations in ciliary genes, particularly for microcephaly, has not been frequently explored. Interestingly, dominant mutations in *KIF2A*, a kinesin involved in both mitotic spindle dynamics and ciliogenesis, were shown to cause MCD through their impact on both cilia and the cell cycle (51). In addition, bilateral agenesis and non-cystic RHD are very rarely reported among the renal phenotypic spectrum of ciliopathies (52). However, a recent report identified a homozygous LOF mutation in IFT27, encoding a component of the intraflagellar transport complex, causes bilateral renal agenesis (53), suggesting that defects in ciliary genes can lead to RHD.

We investigated a potential role for KIF14 in ciliogenesis. We found that, upon overexpression, KIF14 localises to cilia (not shown), but failed to find any evidence for a direct role in ciliogenesis *in vitro*. Intriguingly, the zebrafish embryos harbouring LOF mutations in *kif14* demonstrate ciliopathy phenotypes, but, once again, our analyses failed to identify a direct impact on ciliogenesis *in vivo*. However, we cannot formally exclude its potential role in the transport of cargo into the cilium, which remains to be explored. Based on these results, it is therefore unlikely that a disruption of ciliary function can account for a shared mechanism at the origin of renal and brain developmental defects.

The observation that KIF14-stained midbodies accumulate within the lumen of UB tips in human foetal kidneys provides a key clue to better understand the mechanism by which the loss of KIF14 affects both brain and kidney development in humans. It has previously been shown that midbody remnants are released or ‘secreted’ into the cerebrospinal fluid in mice. This accumulation, during the early stages of brain development, corresponds to the amplification of neural progenitors. During symmetrical division of

these cells, cytokinesis occurs at the apical membrane and midbodies are formed within the lumen, where they are released following abscission (54). In UB tips, mitosis of proliferating UB epithelial cells occurs in the lumen of the expanding/branching tubular structures by a more complex process (36). Dividing cells protrude at the surface of the epithelium, within the lumen, and while one of the daughter cells remains attached to the basal membrane and retracts after mitosis, the other one intercalates between adjacent cells to integrate into the epithelium layer. Subsequently, midbodies are likely formed in the lumen of UB tips, where they could be released and accumulate, as occurs in the brain. To our knowledge, there is no other organ where a similar process resulting in the massive release of midbody remnants has been reported. The fact that both organs are dramatically affected by *KIF14* LOF mutations strongly indicates that KIF14 plays a key role *in vivo* during these 'symmetric' divisions, whereby abscission occurs on both sides of the midbody and leads to their release into the extracellular milieu.

Intriguingly, LOF mutations in CIT lead to mild to severe microcephaly in humans (31–34) which is only occasionally (1 case) found associated with severe kidney defects (32). These observations suggest that KIF14 may play a specific function during kidney development. Recent transcriptomic and single cell transcriptomic analyses revealed expression of mitosis-related genes during the early development of the human kidney (55, 56), including both *CIT* and *KIF14*, as well as other genes known to play crucial roles at the midbody (KIF23, KIF20A, ANLN, etc…). These data suggest that other proteins required for cytokinesis could also have important functions during kidney development and may be able compensate one another, except in the case of KIF14. Compensation mechanisms likely explain why the loss of *Kif14* in the mouse does not lead to kidney defects (28). Of note, a similar lack of kidney phenotypes was previously observed in mouse models for a number of human kidney diseases (8, 57, 58).

The key question for future investigations is: do 'secreted' midbodies have a function or not? Recent work has changed the view of midbodies and midbody remnants from passive structures eliminated after mitosis. Several groups identified possible post-mitotic functions of midbodies when inherited or captured by daughter or neighbouring cells, including cell fate (stemness), polarity or ciliogenesis (22, 59). In the brain, midbody remnants were purified from the ventricular fluid, indicating

that most of them are not immediately recaptured by one of the daughter cells. Their function within the developing brain remains, however, to be determined. The images that we obtained clearly show the accumulation of midbodies in the lumen of UB tips. We cannot exclude that they may remain associated with the apical membrane of the UB tip cells where they could be involved in local signalling events and/or ciliogenesis. However, their localisation in the central part of the lumen in most UB tip profiles suggests that they are released within the lumen, as in the developing brain. In this case, it is tempting to speculate that the connection of these midbody-filled UB tips to a newly formed and functional nephron would result in the expulsion of the midbodies by the incoming filtrate, leading, either, to signalling in the collecting duct, or to elimination in the urine. All these exciting issues remain open and a source of future investigations.

Materials and Methods

Ethics statement

This study was conducted with the approval of the « Comité de Protection des Personnes pour la Recherche Biomédicale Ile de France II ». Approval was obtained under numbers 2007-02-09/DC-2008-229 and 2009-164/DC-2011-1449. For each foetus, written informed consent was obtained from the parents. For studies using animal data: housing and handling of fish were performed in accordance with the guidelines established by the French Council on animal care "Guide for the Care and Use of Laboratory Animals": EEC86/609 Council Directive—Decree 2001–131. The project was approved by the departmental director of "Services Vétérinaires de la Préfecture de Police de Paris" and by the ethical committee of the Paris Descartes University (approval number: A75-15-34).

Genetics analyses, WES and Sanger sequencing

Family 3: Foetuses with severe kidney development defects, possibly associated with extrarenal defects, were collected though MARHEA (Centre de référence des Maladies Rénales Héréditaires de l'enfant et de l'adulte). DNA was extracted from frozen lung biopsies of the two affected foetuses of family 3 and whole exome sequencing was performed using the 50 Mb Agilent SureSelect all exon V3 and a HiSeq2500 (Illumina) sequencer. Sequence data were aligned to the human genome reference sequence (hg19 build) using BWA aligner. Downstream processing was carried out with the Genome Analysis Toolkit (GATK), SAMtools, and Picard (http://www.broadinstitute.org/gatk/guide/topic?name=best-practices). The average coverage was 50, with 93.5% of the targeted regions covered > 15X. Variants were annotated using a software system developed by the Paris Descartes University Bioinformatics Platform, based on the Ensembl (GRCh37/hg19), dbSNP, EVS, 1000 genome, ExAC and GnomAD databases. Variants were then prioritised according to their damaging effect (nonsense, frameshift, acceptor/donor splice site mutations, missense variants predicted to be damaging, and their absence or low frequency in GnomAD

and in our in-house database (> 10 000 exomes). For missense variants, prediction of damaging effects was based on PolyPhen2, Sift, Grantham and CADD scores. According to a suspected autosomal recessive inheritance model, only one gene, *KIF14*, was identified as carrying 2 mutations common to both foetuses. Sanger sequencing in foetuses and parents confirmed compound heterozygosity.

In order to look for additional mutations in *KIF14*, probes covering the 30 exons of the gene were designed and added to a previously described SureSelect panel of 330 genes used for molecular diagnosis of CAKUT cases. *KIF14* mutations identified in foetuses from families 1 and 2 have been briefly described in (12).

Family 4: Patients were included via the AGORA (Aetiologic Research into Genetic and Occupational/environmental Risk factors for Anomalies in children) biobank project. The study protocol was approved by the regional Committee on Research involving Human Subjects (CMO Arnhem/Nijmegen 2006/048). DNA from fibroblasts and (umbilical cord) blood was obtained from foetus 1, 2 and 4 and from blood from both parents. Written informed consent was obtained from both parents for whole genome SNP-array analysis and whole-exome sequencing of DNA from foetus 4 and analysis of skin fibroblasts obtained from foetus 1. Because parents were consanguineous and autosomal recessive inheritance was suspected based on the phenotype, single nucleotide polymorphism (SNP)-array analysis was performed to investigate genes located inside regions of homozygosity. Genomic DNA was extracted from fibroblasts obtained from a skin biopsy from foetus 4 according to standard protocols. Analysis of regions of homozygosity and copy number profiling were performed using the CytoSNP-850K BeadChip SNP-array (Illumina, San Diego, CA, USA) according to standard procedures. SNP-array results were visualised and data analysis was performed using Nexus software version 7 (BioDiscovery, Los Angeles, CA, USA) and the reference Human genome build Feb. 2009 GRCh37/hg19. Results were classified with Cartagenia BENCH software (Cartagenia, Leuven, Belgium).

Whole-exome sequencing (WES) was performed on DNA from foetus 4. Protein coding genes and flanking (splice-site consensus) sequences were captured and enriched using the SureSelectXT Human All Exon V5 capture library (Agilent, Santa Clara, CA, USA) and sequenced in rapid run mode on

the HiSeq 2500 Sequencing system (Illumina, San Diego, CA, USA) at a mean target depth of 100X. The target is defined as all coding exons of UCSC (60)and Ensembl (61) +/- 20bp intron flanks. At this depth ~95% of the target is covered at least 15X. Reads were aligned to the reference Human genome build Feb. 2009 GRCh37/hg19 using BWA (BWA-MEM v0.7.5a) and variants were called using the GATK haplotype caller (v2.7-2). Results were imported into Cartagenia BENCH Lab NGS Module (Cartagenia, Leuven, Belgium) for variant annotation, filtering and prioritisation. Filtering was performed for variants in genes associated with neurodevelopmental abnormalities (for a full list of genes, see Supplementary Methods S1). Identified variants were validated and segregation analysis was performed using standard Sanger sequencing.

Plasmids

Plasmids encoding wild-type KIF14 GFP-fusion and the CCf domain of CIT (429-835aa) fused to mCherry- were kind gifts from F. Barr and S. Narumiya, respectively (18, 21). Variants from the affected foetuses were introduced in the GFP-KIF14 construct using Pfu turbo site-directed mutagenesis as previously described (44). The GST-mKif14 construct (pGex6P1) was described previously (16). Mutant mKIF14-MD-T491M DNA was generated by gene synthesis (Genscript, NJ, USA) and cloned into pGex6P1.

Antibodies

The primary antibodies used were; mouse anti-acetylated α-tubulin (1:10,000, Sigma, T6793), rabbit anti-KIF14 (1:300, Bethyl, A300-233A and A300-912A; 1:1,000, Abcam ab3746), mouse anti-α-Tubulin (1:5000, Sigma, T5168), mouse anti-CRIK (1:500, BD Biosciences, 611376), rabbit anti-SIX2 (1:200, Proteintech, 11562-I-AP), goat anti-PAX2 (1:200, RD System, AF3364), rabbit anti-phospho-histone H3 (1:200, Cell Signalling, #3377S) rabbit anti-GFP (Life Technologies, A-11122), rabbit anti-dsRed (ClonTech, 632496), mouse anti-GAPDH (Millipore, MAB374) and Phalloidin-TRITC (1:300, Sigma, P1951). Cells were incubated with secondary antibodies (Donkey) conjugated to Alexa Fluor® 488, 555

or 647 (Molecular Probes, Invitrogen). Sheep horseradish peroxidase-coupled antibodies were from GE Healthcare (anti-mouse: NA931V; anti-rabbit: NA934V).

Cell Culture

Foetal control- and foetus-derived fibroblasts, human Embryonic Kidney 293 (HEK293) and HeLa cells (ATCC) were cultured in Dulbecco's Modified Eagle Medium, DMEM (Gibco®, Life Technologies) supplemented with 10% Foetal Bovine Serum (FBS, Invitrogen), glutamine and penicillin/streptomycin. Inner Medullary Collective Duct 3 (IMCD3) and hTERT-Retinal Pigment Epithelial (RPE1) cells were cultured in Dulbecco's Modified Eagle Medium, DMEM F:12, (Gibco®, Life Technologies) also supplemented with 10% FBS, glutamine and penicillin/streptomycin. Hela, HEK293 and IMCD3 cells were transfected using Lipofectamine 2000 (Life Technologies, 11668-019) and RPE1 using FuGENE® (Promega, E2311) and maintained in culture for 24 hours.

Biochemistry

Transfected cells were lysed in 0.5% triton, 150mM NaCl and 50mM pH7.5 Tris HCl. For immunoprecipitations, cleared lysates were incubated with mouse isotypic control antibodies and G-protein beads (Sigma, P7700) for 2 hours at 4^{o}C. 1mg of precleared proteins were incubated with mouse monoclonal anti-GFP antibodies (Roche, 11814460001) coupled to G-protein beads for 3 hours at 4^{o}C. Beads were washed three times with increasing amounts of NaCl (150nM, 300nM and 600nM NaCl in 50mM Tris-HCl pH7.5), resuspended in 2x sample buffer (Sigma, S3401) and boiled at 95^{o}C for 5 minutes. For immunoblotting, lysates and immunoprecipitates were separated by polyacrylamide gel electrophoresis (SDS-PAGE) and transferred onto polyvinylidene fluoride transfer membranes (PVDF, GE Healthcare). Immunoblotting was performed using the indicated primary antibodies and revealed using the ECL+ Detection Kit (GE Healthcare).

Microtubule co-sedimentation assay

Recombinant WT and mutant MBP-hKIF14-MD and GST-mKIF14-MD proteins were expressed and purified in the same manner as previously described (16). Microtubule preparation and co-sedimentation assays were performed as previously described (62), with some modifications. Briefly, taxol-stabilised microtubules were prepared by polymerising tubulin at 50 μM in 1×BRB80 (80 mM Pipes pH 6.8, 1 mM EGTA, and 1 mM $MgCl_2$), 1 mM GTP, and 1 mM DTT in the presence of 10% DMSO at 37 °C for 25-30 min, then diluted to 10 μM working stocks in 1× BRB80 containing 20 μM taxol. Binding reactions were performed by mixing 500 nM of the indicated KIF14 constructs with 2 μM taxol-stabilised microtubules in 1×BRB80 supplemented with 25mM KCl, 1 mM DTT, 0.01% Tween-20, and 20 μM taxol. After a 20-min incubation, mixtures were spun at 240,000×*g* for 5 min at 25°C. The supernatant and pellet fractions were recovered and resuspended in Laemmli buffer. Samples were resolved by SDS-PAGE. Gels were stained with Coomassie blue R250 dye, destained, and scanned with a digital scanner.

ATPase activity assay

KIF14 ATPase activity was monitored by a malachite green-based phosphate detection method, as previously described (16). Briefly, reactions were carried out in BRB80-based buffer (80 mM PIPES pH 6.8, 1 mM MgCl2, 1 mM EGTA, 20 μM taxol, 25 mM KCl, 0.25 mg/mL BSA, 1 mM DTT, 0.02% Tween), supplemented with 1 mM ATP, with 2 μM taxol-stabilised microtubules, and 50 nM KIF14 protein constructs. Basal activity of the Kif14 constructs was determined using the same reaction condition without microtubules. Reactions were allowed to proceed for 10 min, quenched with perchloric acid and malachite green reagent. The signal was quantified by measuring the absorbance at 620 nm in a Genios Plus plate reader (Tecan).

CRISPR

Guide couples were designed using CRISPOR and MIT targeting exon 5 of *Kif14* and cloned into Cas9 (nickase) plasmids expressing either GFP or mCherry. The Cas9 nickase encoding plasmid pSpCas9n(BB)-2A-GFP was a gift from Feng Zhang (Addgene plasmid # 48140; (63)). It was modified to

generate an mCherry version. Briefly, the cleavable peptide 2A (P2A) sequence was cloned upstream of mCherry (cold fusion cloning kit, System Biosciences) and a BbsI/BpiI restriction site was mutated (Quick Change kit, Stratagene) as it was interfering with sgRNA subcloning in the final desired mCherry vectors. The recipient vector pSpCas9n(BB)-2A-GFP (# 48140) was digested with EcoRI to excise the GFP, which was replaced by the P2A-mCherry insert. The sequences of the guides used were; #4-GFP: AGTGTCCACTCGCCAGCGTGAGG and #17-mCherry: ATTGACAGGCCTTCAACATACGG. IMCD3 cells were co-transfected with the GFP and mCherry vectors, sorted by flow cytometry for green and red fluorescence and clones were isolated. Nuclear DNA was extracted using QuickExtract™ DNA Extraction Solution (Tebu-bio, QE09050), and Sanger sequenced using the following primers; forward $^{5'}$gcacatctcgtgagaac$^{3'}$ and reverse $^{5'}$gaacaaagaactaagagccc$^{3'}$.

Immunofluorescence

Cells were cultured on cover slips and fixed in 4% paraformaldehyde. Primary antibody incubation was performed in Dulbecco's phosphate buffered saline (PBS, Sigma), 0.1% Triton-X-100 (Sigma) and 1 mg/ml or 3% bovine serum albumin (BSA, Sigma). After 3 washes with the incubation buffer, cells were incubated with secondary antibodies (1:300) in PBS-BSA (1mg/ml) and after 3 washes in PBS, nuclei stained using Hoechst (#33342, Sigma). Coverslips were mounted onto glass slides using Mowiol® 4-88 (Sigma).

Frozen tissues from control and affected kidneys were sectioned (8µm) using a Leica microtome. Melted sections were postfixed in acetone (10 minutes, room temperature). The slides were washed twice in PBS and then blocked for 45 minutes at 4°C in 10% normal donkey serum diluted in PBT (PBS, 0.1% Tween) and then incubated with the primary antibodies diluted in PBT (overnight, 4°C). After 3 washes in PBT, sections were incubated with secondary antibodies diluted in PBT and, after two washes in PBS, nuclei stained using Hoechst (#33342, Sigma) and finally mounted onto glass slides using Mowiol® 4-88 (Sigma) or Fluormount G (Cell Lab, Beckman Coulter, Brea, CA, US).

Stained cells and tissues were imaged using an epi-illumination microscope (DMR, Leica) with a cooled charge-coupled device (CCD) camera (Leica DFC3000G). Images were acquired with LAS (Leica V4.6) and processed with ImageJ and Photoshop CS2 (Adobe Systems Inc., San Jose, CA, USA). Confocal imaging was performed to acquire stainings of foetal fibroblasts using a Zeiss Confocal laser microscope LSM700 and images were processed with ZEN 2011 software.

Zebrafish Experiments

The zebrafish *kif14* mutant line sa24165 was acquired from the Zebrafish Mutation Project (Sanger Institute) and maintained at 28.5^{o}C under standard conditions and according to European Law. *Kif14*$^{+/-}$ zebrafish were crossed with *Tg(βactin:arl13bGFP)*, *Tg(wt1b:GFP)* and *Tg(cldnB:lynGFP)* to allow analysis of cilia (43), proximal (41) and distal pronephros (47), respectively. Genotyping was performed by placing embryos in 10mM Tris pH8.0, 1mM EDTA and 1.2mg/ml at 55^{o}C overnight, and the reaction was stopped by incubating at 95^{o}C for 5 minutes. DNA from exon 11 was Sanger sequenced using the following primers: forward $^{5'}$gtgtgagattcgagtgttttc$^{3'}$ and reverse $^{5'}$gttgcatatttaaacggaatg$^{3'}$.

Live embryos were analysed using a Leica M165FC stereoscope. For immunofluorescence, embryos were fixed in 4% PFA, washed in PBS and blocked in PBS, 0.3% Triton and 4% BSA. Both primary and secondary antibody incubations were performed overnight at 4^{o}C. Fixed and stained embryos were stored in Mowiol and mounted in 1% low gelling temperature agarose (Sigma, A9414) and imaged using a Zeiss Axio Observer Z1 inverted microscope equipped with a Yokogawa CSU-X1 spinning disk. Images were acquired with a 40x water immersion objective (1.46) through a Hamamatsu Orca Flash 4.0 sCMOS Camera. Images were processed using ImageJ and Photoshop CS2 (Adobe Systems Inc., San Jose, CA, USA).

Acknowledgements

We are grateful to the families for their participation. We greatly acknowledge N. Goudin and M Garfa-Traoré (Necker cell imaging facility) for providing expert knowledge on confocal microscopy, members of the Bioinformatic and Genomic facilities of the Imagine Institute, and C. Arrondelle and F. Legendre for their help on tissue sections and immnunohistochemistry. We acknowledge E.D. Peters for immunofluorescence experiments. We would like to thank F. Barr, U. Gruneberg, S. Angers and S. Narumiya for their generous gifts of KIF14 and Citron Kinase encoding plasmids. This work was supported by the Fondation pour la Recherche Médicale (DEQ20130326532 to SS); the European Union's Seventh Framework Programme (FP7/2007–2013) grant 305608 (EURenOmics, CJ); the GIS-Institut des Maladies Rares (AMA11025KSA to CJ and SS); the CIHR, NSERC, CCSRI, and FRQS (BK); the Swiss National Science Foundation (SNSF, IF); the Dutch Kidney Foundation KOUNCIL consortium (CP11.18). The Imagine Institute is supported by an ANR grant (ANR-A0-IAHU-01). We acknowledge the Imagine Institute for the purchase of Leica SP8 STED and Zeiss Spinning Disk microscopes, and the Fondation ARC (EML20110602384) for the purchase of the LEICA SP8 confocal microscope.

Conflict of Interest Statement: None declared

References:

1. Nicolaou,N., Renkema,K.Y., Bongers,E.M.H.F., Giles,R.H. and Knoers,N.V.A.M. (2015) Genetic, environmental, and epigenetic factors involved in CAKUT. *Nat. Rev. Nephrol.*, **11**, 720–731.

2. Braun,D.A. and Hildebrandt,F. (2017) Ciliopathies. *Cold Spring Harb. Perspect. Biol.*, **9**.

3. McMahon,A.P. (2016) Development of the Mammalian Kidney. *Curr. Top. Dev. Biol.*, **117**, 31–64.

4. Seely,J.C. (2017) A brief review of kidney development, maturation, developmental abnormalities, and drug toxicity: juvenile animal relevancy. *J. Toxicol. Pathol.*, **30**, 125–133.

5. Drummond,I.A. and Davidson,A.J. (2016) Zebrafish kidney development. *Methods Cell Biol.*, **134**, 391–429.

6. Poureetezadi,S.J. and Wingert,R.A. (2016) Little fish, big catch: zebrafish as a model for kidney disease. *Kidney Int.*, **89**, 1204–1210.

7. Uy,N. and Reidy,K. (2016) Developmental Genetics and Congenital Anomalies of the Kidney and Urinary Tract. *J. Pediatr. Genet.*, **5**, 51–60.

8. Barak,H., Huh,S.-H., Chen,S., Jeanpierre,C., Martinovic,J., Parisot,M., Bole-Feysot,C., Nitschké,P., Salomon,R., Antignac,C., *et al.* (2012) FGF9 and FGF20 maintain the stemness of nephron progenitors in mice and man. *Dev. Cell*, **22**, 1191–1207.

9. De Tomasi,L., David,P., Humbert,C., Silbermann,F., Arrondel,C., Tores,F., Fouquet,S., Desgrange,A., Niel,O., Bole-Feysot,C., *et al.* (2017) Mutations in GREB1L Cause Bilateral Kidney Agenesis in Humans and Mice. *Am. J. Hum. Genet.*, **101**, 803–814.

10. Humbert,C., Silbermann,F., Morar,B., Parisot,M., Zarhrate,M., Masson,C., Tores,F., Blanchet,P., Perez,M.-J., Petrov,Y., *et al.* (2014) Integrin alpha 8 recessive mutations are responsible for bilateral renal agenesis in humans. *Am. J. Hum. Genet.*, **94**, 288–294.

11. Filges,I., Nosova,E., Bruder,E., Tercanli,S., Townsend,K., Gibson,W.T., Röthlisberger,B., Heinimann,K., Hall,J.G., Gregory-Evans,C.Y., *et al.* (2014) Exome sequencing identifies mutations in KIF14 as a novel cause of an autosomal recessive lethal fetal ciliopathy phenotype. *Clin. Genet.*, **86**, 220–228.

12. Heidet,L., Morinière,V., Henry,C., De Tomasi,L., Reilly,M.L., Humbert,C., Alibeu,O., Fourrage,C., Bole-Feysot,C., Nitschké,P., *et al.* (2017) Targeted Exome Sequencing Identifies PBX1 as Involved in Monogenic Congenital Anomalies of the Kidney and Urinary Tract. *J. Am. Soc. Nephrol. JASN*, **28**, 2901–2914.

13. Paridaen,J.T.M.L. and Huttner,W.B. (2014) Neurogenesis during development of the vertebrate central nervous system. *EMBO Rep.*, **15**, 351–364.

14. Romero,D.M., Bahi-Buisson,N. and Francis,F. (2018) Genetics and mechanisms leading to human cortical malformations. *Semin. Cell Dev. Biol.*, **76**, 33–75.

15. Verhey,K.J., Kaul,N. and Soppina,V. (2011) Kinesin assembly and movement in cells. *Annu. Rev. Biophys.*, **40**, 267–288.

16. Arora,K., Talje,L., Asenjo,A.B., Andersen,P., Atchia,K., Joshi,M., Sosa,H., Allingham,J.S. and Kwok,B.H. (2014) KIF14 Binds Tightly to Microtubules and Adopts a Rigor-Like Conformation. *J. Mol. Biol.*, **426**, 2997–3015.

17. Carleton,M., Mao,M., Biery,M., Warrener,P., Kim,S., Buser,C., Marshall,C.G., Fernandes,C., Annis,J. and Linsley,P.S. (2006) RNA interference-mediated silencing of mitotic kinesin KIF14 disrupts cell cycle progression and induces cytokinesis failure. *Mol. Cell. Biol.*, **26**, 3853–3863.

18. Gruneberg,U., Neef,R., Li,X., Chan,E.H.Y., Chalamalasetty,R.B., Nigg,E.A. and Barr,F.A. (2006) KIF14 and citron kinase act together to promote efficient cytokinesis. *J. Cell Biol.*, **172**, 363–372.

19. D'Avino,P.P., Giansanti,M.G. and Petronczki,M. (2015) Cytokinesis in animal cells. *Cold Spring Harb. Perspect. Biol.*, **7**, a015834.

20. Bassi,Z.I., Audusseau,M., Riparbelli,M.G., Callaini,G. and D'Avino,P.P. (2013) Citron kinase controls a molecular network required for midbody formation in cytokinesis. *Proc. Natl. Acad. Sci. U. S. A.*, **110**, 9782–9787.

21. Watanabe,S., De Zan,T., Ishizaki,T. and Narumiya,S. (2013) Citron kinase mediates transition from constriction to abscission through its coiled-coil domain. *J. Cell Sci.*, **126**, 1773–1784.

22. Dionne,L.K., Wang,X.-J. and Prekeris,R. (2015) Midbody: from cellular junk to regulator of cell polarity and cell fate. *Curr. Opin. Cell Biol.*, **35**, 51–58.

23. Ahmed,S.M., Thériault,B.L., Uppalapati,M., Chiu,C.W.N., Gallie,B.L., Sidhu,S.S. and Angers,S. (2012) KIF14 negatively regulates Rap1a-Radil signaling during breast cancer progression. *J. Cell Biol.*, **199**, 951–967.

24. Alphey,L., Parker,L., Hawcroft,G., Guo,Y., Kaiser,K. and Morgan,G. (1997) KLP38B: a mitotic kinesin-related protein that binds PP1. *J. Cell Biol.*, **138**, 395–409.

25. Molina,I., Baars,S., Brill,J.A., Hales,K.G., Fuller,M.T. and Ripoll,P. (1997) A chromatin-associated kinesin-related protein required for normal mitotic chromosome segregation in Drosophila. *J. Cell Biol.*, **139**, 1361–1371.

26. Ohkura,H., Török,T., Tick,G., Hoheisel,J., Kiss,I. and Glover,D.M. (1997) Mutation of a gene for a Drosophila kinesin-like protein, Klp38B, leads to failure of cytokinesis. *J. Cell Sci.*, **110 (Pt 8)**, 945–954.

27. Ruden,D.M., Cui,W., Sollars,V. and Alterman,M. (1997) A Drosophila kinesin-like protein, Klp38B, functions during meiosis, mitosis, and segmentation. *Dev. Biol.*, **191**, 284–296.

28. Fujikura,K., Setsu,T., Tanigaki,K., Abe,T., Kiyonari,H., Terashima,T. and Sakisaka,T. (2013) Kif14 mutation causes severe brain malformation and hypomyelination. *PloS One*, **8**, e53490.

29. Makrythanasis,P., Maroofian,R., Stray-Pedersen,A., Musaev,D., Zaki,M.S., Mahmoud,I.G., Selim,L., Elbadawy,A., Jhangiani,S.N., Coban Akdemir,Z.H., *et al.* (2018) Biallelic variants in KIF14 cause intellectual disability with microcephaly. *Eur. J. Hum. Genet. EJHG*, **26**, 330–339.

30. Moawia,A., Shaheen,R., Rasool,S., Waseem,S.S., Ewida,N., Budde,B., Kawalia,A., Motameny,S., Khan,K., Fatima,A., *et al.* (2017) Mutations of KIF14 cause primary microcephaly by impairing cytokinesis. *Ann. Neurol.*, **82**, 562–577.

31. Basit,S., Al-Harbi,K.M., Alhijji,S.A.M., Albalawi,A.M., Alharby,E., Eldardear,A. and Samman,M.I. (2016) CIT, a gene involved in neurogenic cytokinesis, is mutated in human primary microcephaly. *Hum. Genet.*, **135**, 1199–1207.

32. Harding,B.N., Moccia,A., Drunat,S., Soukarieh,O., Tubeuf,H., Chitty,L.S., Verloes,A., Gressens,P., El Ghouzzi,V., Joriot,S., *et al.* (2016) Mutations in Citron Kinase Cause Recessive Microlissencephaly with Multinucleated Neurons. *Am. J. Hum. Genet.*, **99**, 511–520.

33. Li,H., Bielas,S.L., Zaki,M.S., Ismail,S., Farfara,D., Um,K., Rosti,R.O., Scott,E.C., Tu,S., Chi,N.C., *et al.* (2016) Biallelic Mutations in Citron Kinase Link Mitotic Cytokinesis to Human Primary Microcephaly. *Am. J. Hum. Genet.*, **99**, 501–510.

34. Shaheen,R., Hashem,A., Abdel-Salam,G.M.H., Al-Fadhli,F., Ewida,N. and Alkuraya,F.S. (2016) Mutations in CIT, encoding citron rho-interacting serine/threonine kinase, cause severe primary microcephaly in humans. *Hum. Genet.*, **135**, 1191–1197.

35. Kapoor,T.M. and Mitchison,T.J. (1999) Allele-specific activators and inhibitors for kinesin. *Proc. Natl. Acad. Sci. U. S. A.*, **96**, 9106–9111.

36. Packard,A., Georgas,K., Michos,O., Riccio,P., Cebrian,C., Combes,A.N., Ju,A., Ferrer-Vaquer,A., Hadjantonakis,A.-K., Zong,H., *et al.* (2013) Luminal mitosis drives epithelial cell dispersal within the branching ureteric bud. *Dev. Cell*, **27**, 319–330.

37. Kettleborough,R.N.W., Busch-Nentwich,E.M., Harvey,S.A., Dooley,C.M., de Bruijn,E., van Eeden,F., Sealy,I., White,R.J., Herd,C., Nijman,I.J., *et al.* (2013) A systematic genome-wide analysis of zebrafish protein-coding gene function. *Nature*, **496**, 494–497.

38. Lowery,L.A. and Sive,H. (2005) Initial formation of zebrafish brain ventricles occurs independently of circulation and requires the nagie oko and snakehead/atp1a1a.1 gene products. *Dev. Camb. Engl.*, **132**, 2057–2067.

39. Novorol,C., Burkhardt,J., Wood,K.J., Iqbal,A., Roque,C., Coutts,N., Almeida,A.D., He,J., Wilkinson,C.J. and Harris,W.A. (2013) Microcephaly models in the developing zebrafish retinal neuroepithelium point to an underlying defect in metaphase progression. *Open Biol.*, **3**, 130065–130065.

40. Marra,A.N., Li,Y. and Wingert,R.A. (2016) Antennas of organ morphogenesis: the roles of cilia in vertebrate kidney development. *Genes. N. Y. N 2000*, **54**, 457–469.

41. Perner,B., Englert,C. and Bollig,F. (2007) The Wilms tumor genes wt1a and wt1b control different steps during formation of the zebrafish pronephros. *Dev. Biol.*, **309**, 87–96.

42. Lundberg,Y.W., Xu,Y., Thiessen,K.D. and Kramer,K.L. (2015) Mechanisms of otoconia and otolith development. *Dev. Dyn. Off. Publ. Am. Assoc. Anat.*, **244**, 239–253.

43. Borovina,A., Superina,S., Voskas,D. and Ciruna,B. (2010) Vangl2 directs the posterior tilting and asymmetric localization of motile primary cilia. *Nat. Cell Biol.*, **12**, 407–412.

44. Bizet,A.A., Becker-Heck,A., Ryan,R., Weber,K., Filhol,E., Krug,P., Halbritter,J., Delous,M., Lasbennes,M.-C., Linghu,B., *et al.* (2015) Mutations in TRAF3IP1/IFT54 reveal a new role for IFT proteins in microtubule stabilization. *Nat. Commun.*, **6**, 8666.

45. Burcklé,C., Gaudé,H.-M., Vesque,C., Silbermann,F., Salomon,R., Jeanpierre,C., Antignac,C., Saunier,S. and Schneider-Maunoury,S. (2011) Control of the Wnt pathways by nephrocystin-4 is required for morphogenesis of the zebrafish pronephros. *Hum. Mol. Genet.*, **20**, 2611–2627.

46. Basten,S.G. and Giles,R.H. (2013) Functional aspects of primary cilia in signaling, cell cycle and tumorigenesis. *Cilia*, **2**, 6.

47. Haas,P. and Gilmour,D. (2006) Chemokine signaling mediates self-organizing tissue migration in the zebrafish lateral line. *Dev. Cell*, **10**, 673–680.

48. Vasilyev,A., Liu,Y., Hellman,N., Pathak,N. and Drummond,I.A. (2012) Mechanical stretch and PI3K signaling link cell migration and proliferation to coordinate epithelial tubule morphogenesis in the zebrafish pronephros. *PloS One*, **7**, e39992.

49. Cooperstone,B.G., Friedman,A. and Kaplan,B.S. (1993) Galloway-Mowat syndrome of abnormal gyral patterns and glomerulopathy. *Am. J. Med. Genet.*, **47**, 250–254.

50. Sanna-Cherchi,S., Westland,R., Ghiggeri,G.M. and Gharavi,A.G. (2018) Genetic basis of human congenital anomalies of the kidney and urinary tract. *J. Clin. Invest.*, **128**, 4–15.

51. Broix,L., Asselin,L., Silva,C.G., Ivanova,E.L., Tilly,P., Gilet,J.G., Lebrun,N., Jagline,H., Muraca,G., Saillour,Y., *et al.* (2018) Ciliogenesis and cell cycle alterations contribute to KIF2A-related malformations of cortical development. *Hum. Mol. Genet.*, **27**, 224–238.

52. Grampa,V., Delous,M., Zaidan,M., Odye,G., Thomas,S., Elkhartoufi,N., Filhol,E., Niel,O., Silbermann,F., Lebreton,C., *et al.* (2016) Novel NEK8 Mutations Cause Severe Syndromic Renal Cystic Dysplasia through YAP Dysregulation. *PLoS Genet.*, **12**, e1005894.

53. Quélin,C., Loget,P., Boutaud,L., Elkhartoufi,N., Milon,J., Odent,S., Fradin,M., Demurger,F., Pasquier,L., Thomas,S., *et al.* (2018) Loss of function IFT27 variants associated with an unclassified lethal fetal ciliopathy with renal agenesis. *Am. J. Med. Genet. A.*, 10.1002/ajmg.a.38685.

54. Dubreuil,V., Marzesco,A.-M., Corbeil,D., Huttner,W.B. and Wilsch-Bräuninger,M. (2007) Midbody and primary cilium of neural progenitors release extracellular membrane particles enriched in the stem cell marker prominin-1. *J. Cell Biol.*, **176**, 483–495.

55. Lindström,N.O., McMahon,J.A., Guo,J., Tran,T., Guo,Q., Rutledge,E., Parvez,R.K., Saribekyan,G., Schuler,R.E., Liao,C., *et al.* (2018) Conserved and Divergent Features of Human and Mouse Kidney Organogenesis. *J. Am. Soc. Nephrol. JASN*, **29**, 785–805.

56. Lindström,N.O., De Sena Brandine,G., Tran,T., Ransick,A., Suh,G., Guo,J., Kim,A.D., Parvez,R.K., Ruffins,S.W., Rutledge,E.A., *et al.* (2018) Progressive Recruitment of Mesenchymal Progenitors Reveals a Time-Dependent Process of Cell Fate Acquisition in Mouse and Human Nephrogenesis. *Dev. Cell*, **45**, 651-660.e4.

57. Jiang,S.-T., Chiou,Y.-Y., Wang,E., Lin,H.-K., Lee,S.-P., Lu,H.-Y., Wang,C.-K.L., Tang,M.-J. and Li,H. (2008) Targeted disruption of Nphp1 causes male infertility due to defects in the later steps of sperm morphogenesis in mice. *Hum. Mol. Genet.*, **17**, 3368–3379.

58. Won,J., Marín de Evsikova,C., Smith,R.S., Hicks,W.L., Edwards,M.M., Longo-Guess,C., Li,T., Naggert,J.K. and Nishina,P.M. (2011) NPHP4 is necessary for normal photoreceptor ribbon

synapse maintenance and outer segment formation, and for sperm development. *Hum. Mol. Genet.*, **20**, 482–496.

59. Bernabé-Rubio,M., Andrés,G., Casares-Arias,J., Fernández-Barrera,J., Rangel,L., Reglero-Real,N., Gershlick,D.C., Fernández,J.J., Millán,J., Correas,I., *et al.* (2016) Novel role for the midbody in primary ciliogenesis by polarized epithelial cells. *J. Cell Biol.*, 10.1083/jcb.201601020.

60. Kent,W.J., Sugnet,C.W., Furey,T.S., Roskin,K.M., Pringle,T.H., Zahler,A.M. and Haussler,D. (2002) The human genome browser at UCSC. *Genome Res.*, **12**, 996–1006.

61. Aken,B.L., Achuthan,P., Akanni,W., Amode,M.R., Bernsdorff,F., Bhai,J., Billis,K., Carvalho-Silva,D., Cummins,C., Clapham,P., *et al.* (2017) Ensembl 2017. *Nucleic Acids Res.*, **45**, D635–D642.

62. Solinet,S., Mahmud,K., Stewman,S.F., Ben El Kadhi,K., Decelle,B., Talje,L., Ma,A., Kwok,B.H. and Carreno,S. (2013) The actin-binding ERM protein Moesin binds to and stabilizes microtubules at the cell cortex. *J. Cell Biol.*, **202**, 251–260.

63. Ran,F.A., Hsu,P.D., Wright,J., Agarwala,V., Scott,D.A. and Zhang,F. (2013) Genome engineering using the CRISPR-Cas9 system. *Nat. Protoc.*, **8**, 2281–2308.

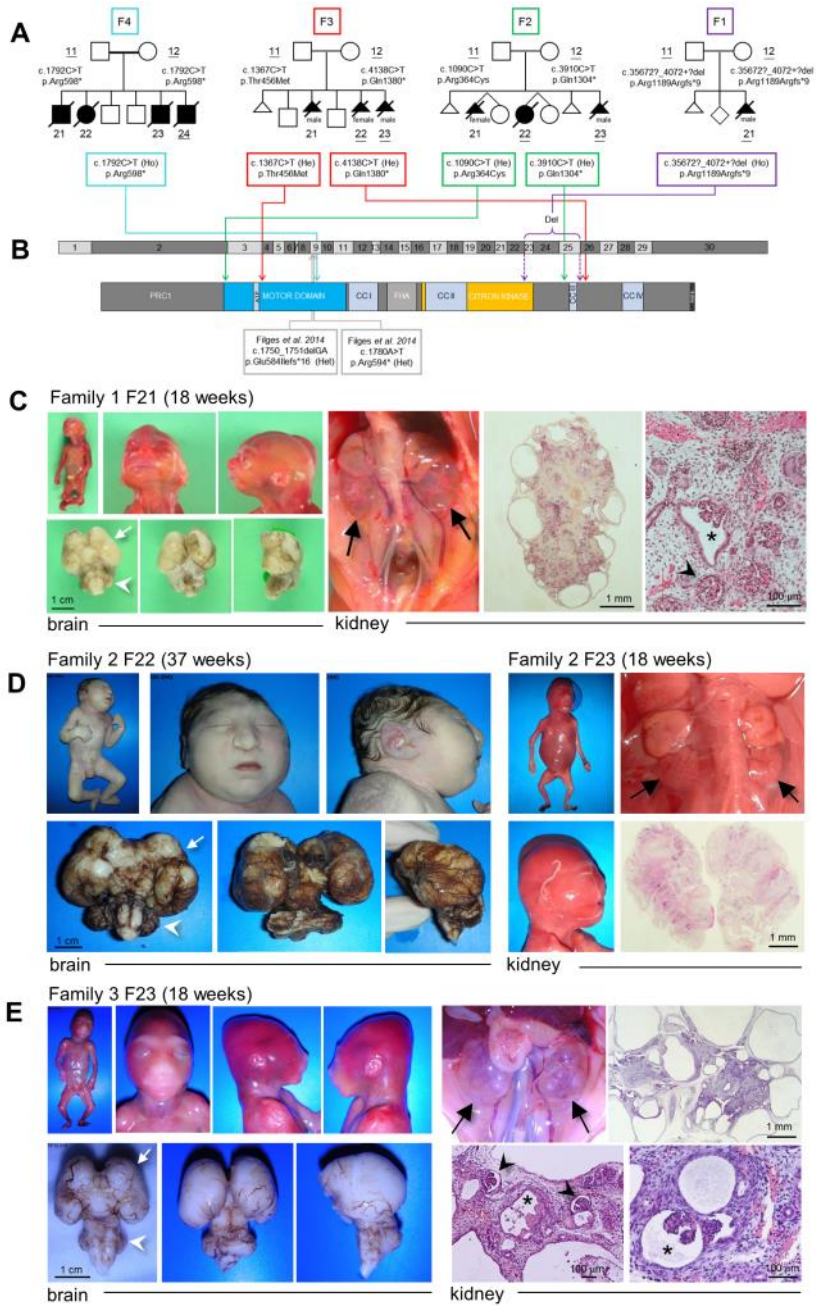

Figure 1. Identification of mutations in *KIF14* in a lethal, foetal syndrome associating severe microcephaly with bilateral renal agenesis, or renal hypodysplasia. (A) Pedigrees of the identified families (F1-4) with homozygous or compound heterozygous mutations in *KIF14*. (B) Schematic representation of *KIF14* cDNA (exons) and protein showing the position of the identified mutations. The PRC1 and Citron Kinase (CIT) binding domains are shown, along with the motor, Fork Head Associated (FHA) and the four coiled-coil (CC I-IV) domains. The compound heterozygous mutations of the previously identified family are also shown (Filges, 2014). Abbreviations: heterozygous (he), homozygous (ho). (C) Foetus 21 of family 1 (18 weeks gestation), pictures of brains and kidneys with representative histological sections from one kidney. (D) Foetus 22 (37 weeks gestation), and foetus 23 (18 weeks) from family 2, pictures of brains and kidneys along with histology of F23 kidneys. (E) Foetus F23 of family 3 (18 weeks gestation), pictures of brain and kidneys along with kidney histology. Black arrows highlight kidneys, black arrowheads glomeruli, asterisks cystic glomeruli, white arrows telencephalon and white arrowheads cerebellum.

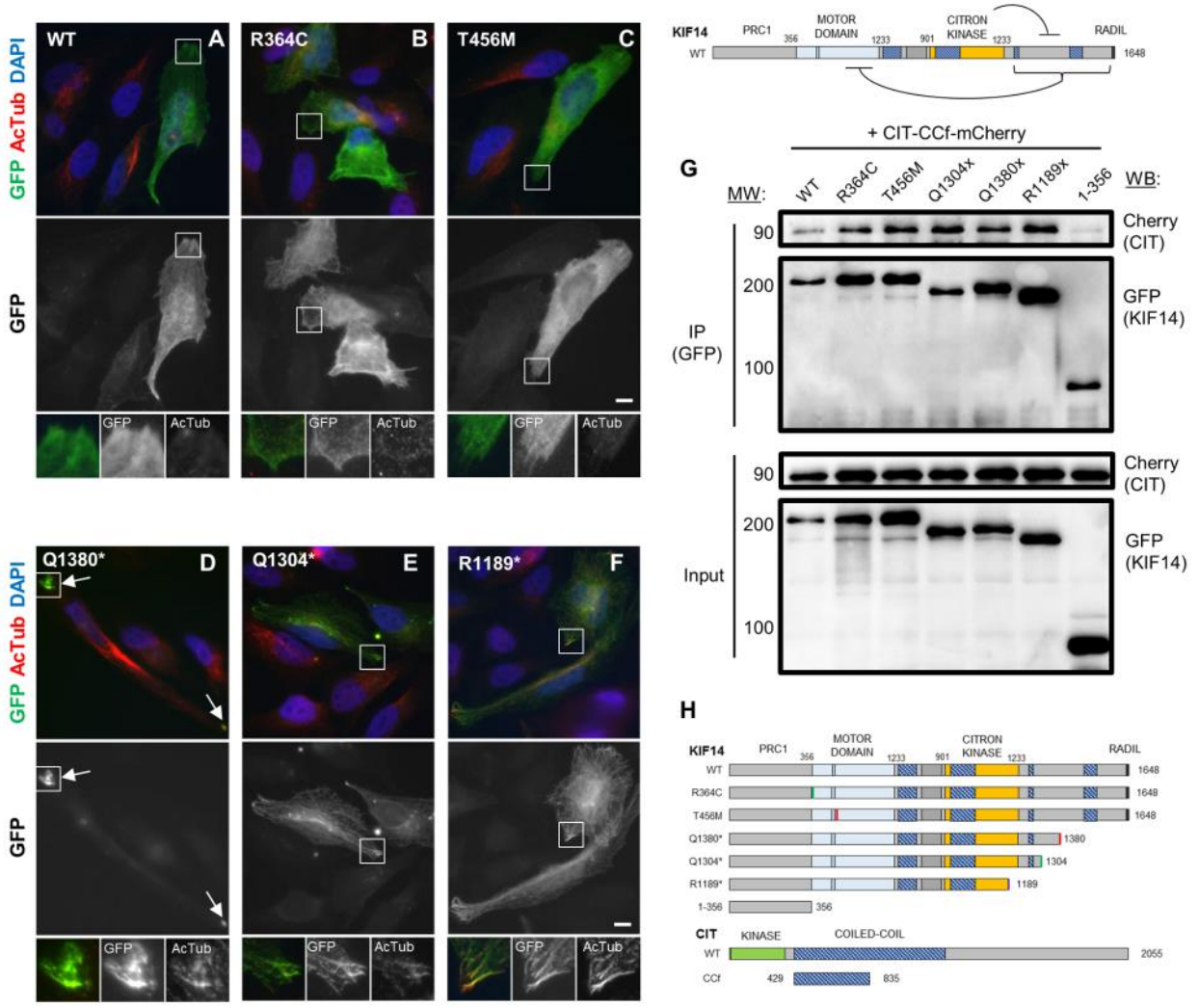

Figure 2. C-terminally truncated variant KIF14 proteins are constitutively targeted to microtubules without impairing CIT binding. (A-F) Immunofluorescence of HeLa cells transfected with a GFP-fusion encoding wild-type or mutant KIF14 GFP fusions. Stable microtubules were stained using an antibody against acetylated-α-tubulin (AcTub; red), and nuclei using Hoechst (blue). Merge colour pictures (top panels) and black and white pictures corresponding to GFP fusions (KIF14; bottom panels) are shown. Scale bars: 5 µm. (G) Lysates from HEK293 cells co-transfected with plasmids encoding GFP-fusions of WT or mutant KIF14 and with an mCherry-fusion of the KIF14 binding domain of CIT (CCf) were immunoprecipitated using an anti-GFP antibody. Lysates and immunoprecipitated proteins were analysed through Western blotting, using antibodies against GFP (KIF14) or mCherry (CIT-CCf). (H) Schematic representation of the constructs used in immunofluorescence and co-immunoprecipitation experiments.

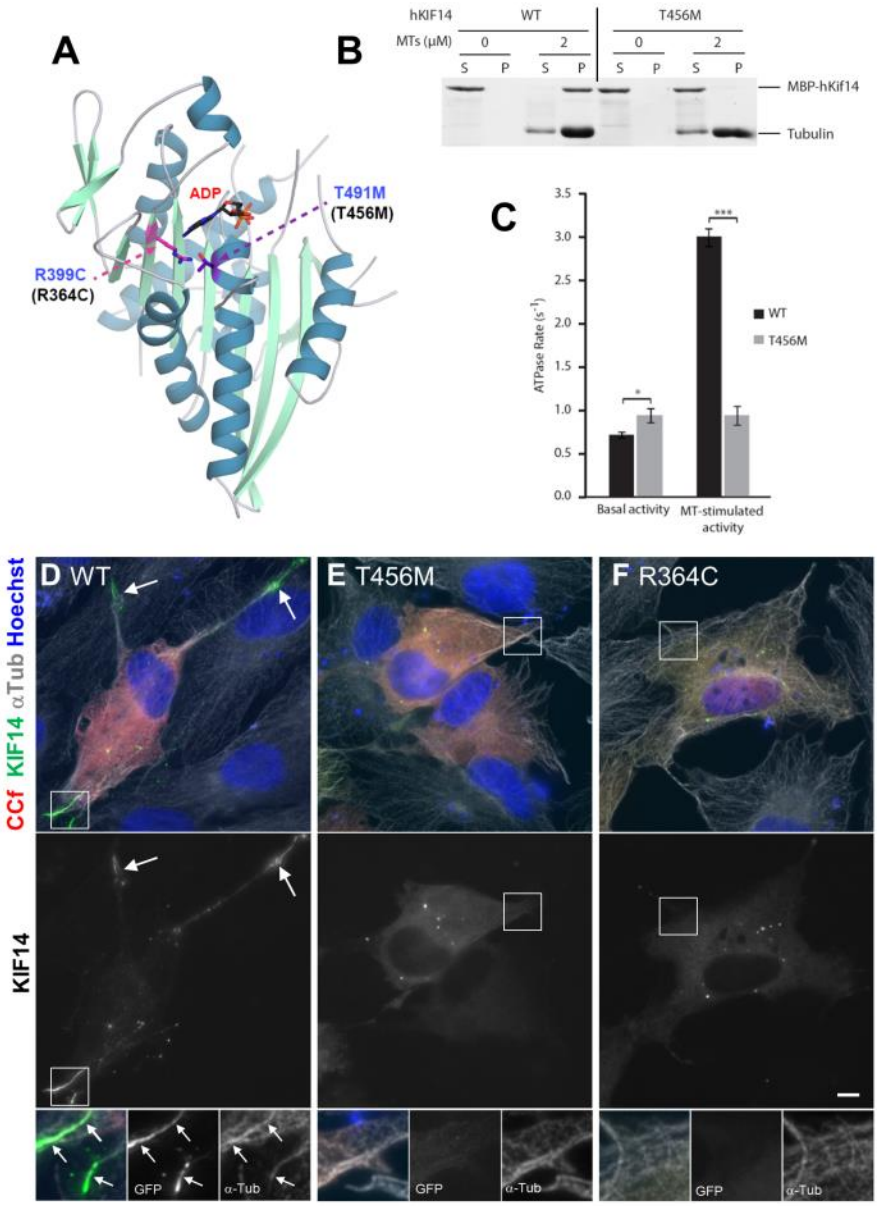

Figure 3. Identified motor domain mutations affect KIF14 activity and impair microtubule binding. (A) Structure of mouse KIF14-MD is shown (PDB ID: 4OZQ ; Arora et al. 2014) with the mutated residues labelled (mouse residues in blue and the corresponding human residues in black). This image was produced in PyMol (The PyMOL Molecular Graphics System, Version 2.0 Schrödinger, LLC). (B) The microtubule-binding activity of human KIF14 motor construct (MBP-hKIF14) was assessed in an ultracentrifugation-based co-sedimentation assay. A representative coomassie blue-stained gel, from four independent experiments, is shown. KIF14 motor constructs and tubulin are indicated. S, supernatant; P, pellet; MT, microtubules. (C) Basal and MT-stimulated ATPase activities of a KIF14 motor construct (MBP-hKIF14) were shown. Data from 4 independent experiments. Error bars, S.D.. Statistics: * $p \leq 0.05$; *** $p \leq 0.001$; by Student's T-test. (D-F) Immunofluorescence of RPE1 cells co-transfected with plasmids encoding GFP-fusion of WT (D) or mutant KIF14 (T456M (E) or R364C (F)), along with an mCherry-fusion of the KIF14 binding domain of CIT (CCf, red) stained for alpha-tubulin (Grey). Merge colour pictures (top panels) and black and white pictures corresponding to GFP fusions (KIF14; bottom panels) are shown. White arrows stress colocasition of KIF14 and α-tubulin. Nuclei were stained using Hoechst (blue). Scale bars: 5 µm.

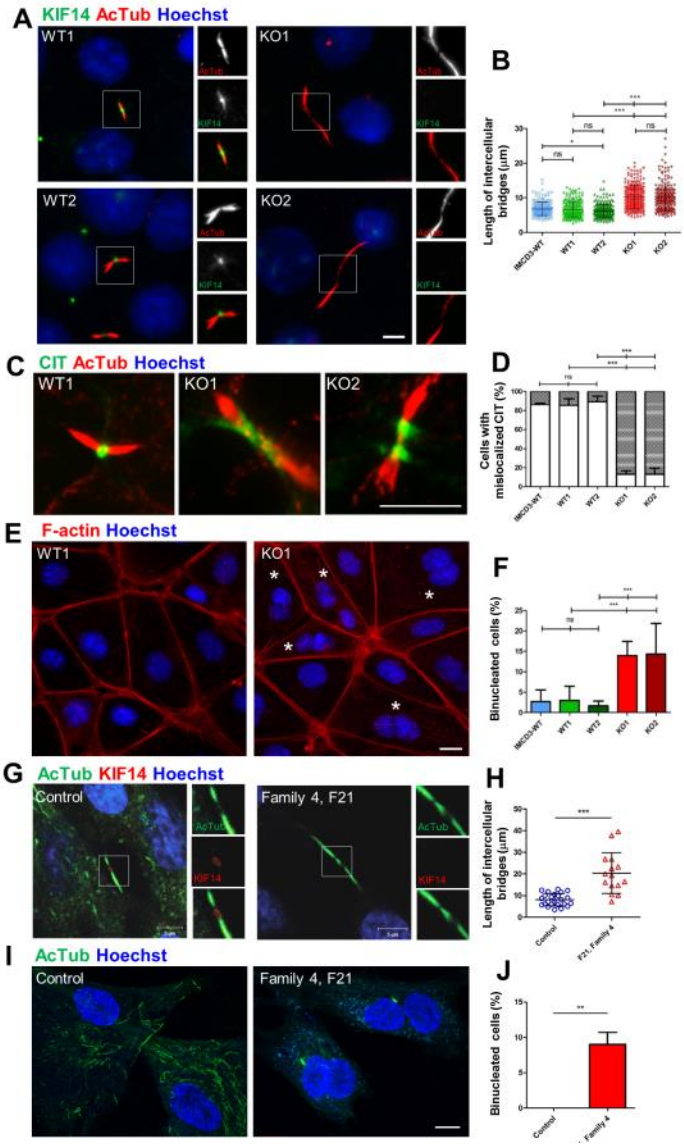

Figure 4. Loss of *Kif14* leads to cytokinesis defects in mIMCD3 cells and in cells from the affected foetuses. (A,B) Cycling Kif14 wild-type (WT1, WT2) and knockout (KO1, KO2) mIMCD3 clones were stained for KIF14 (green), acetylated-α-tubulin (AcTub, red) and DNA (Hoechst, blue). Insets show higher magnification of intercellular bridges stained with AcTub. Length of intercellular bridges in parental IMCD3 cells (IMCD3 WT) and WT and KO clones were quantified using ImageJ (B), as described in materials and methods. (C,D) WT and KO clones were immunostained for CIT (green) and AcTub (red) (C) to quantify the localisation of CIT to the midbody expressed as the percentage of cells with a "normal" single ring CIT staining (D). (E,F) WT and KO clones were stained for F-actin using phalloidin (red), and nuclei using Hoechst (blue) in order to identify (Asterisks, E) and quantify the percentage of binucleated cells (F). (G-J) Fibroblasts derived from control and foetus 24 from family 4 were stained for either acetylated α-tubulin (green) and KIF14 (red; G) or acetylated α-tubulin (green) only (I), as well as for DNA (Hoechst, blue). Length of mitotic bridges (H) and percentage of binucleated (J) were quantified based on these stainings. ns = not significant, **P< 0.001 ***P< 0.0001 from n=3 independent experiments (except in H (n=2)), Dunn's Multiple Comparison Test following the Kruskal-Wallis ANOVA test for length of intercellular bridges (B, H), and Fischer's exact test for CIT localisation and binucleated cells (D, F, J). Scale bars: 5 µm (A, C, E and G), 10 µm (I).

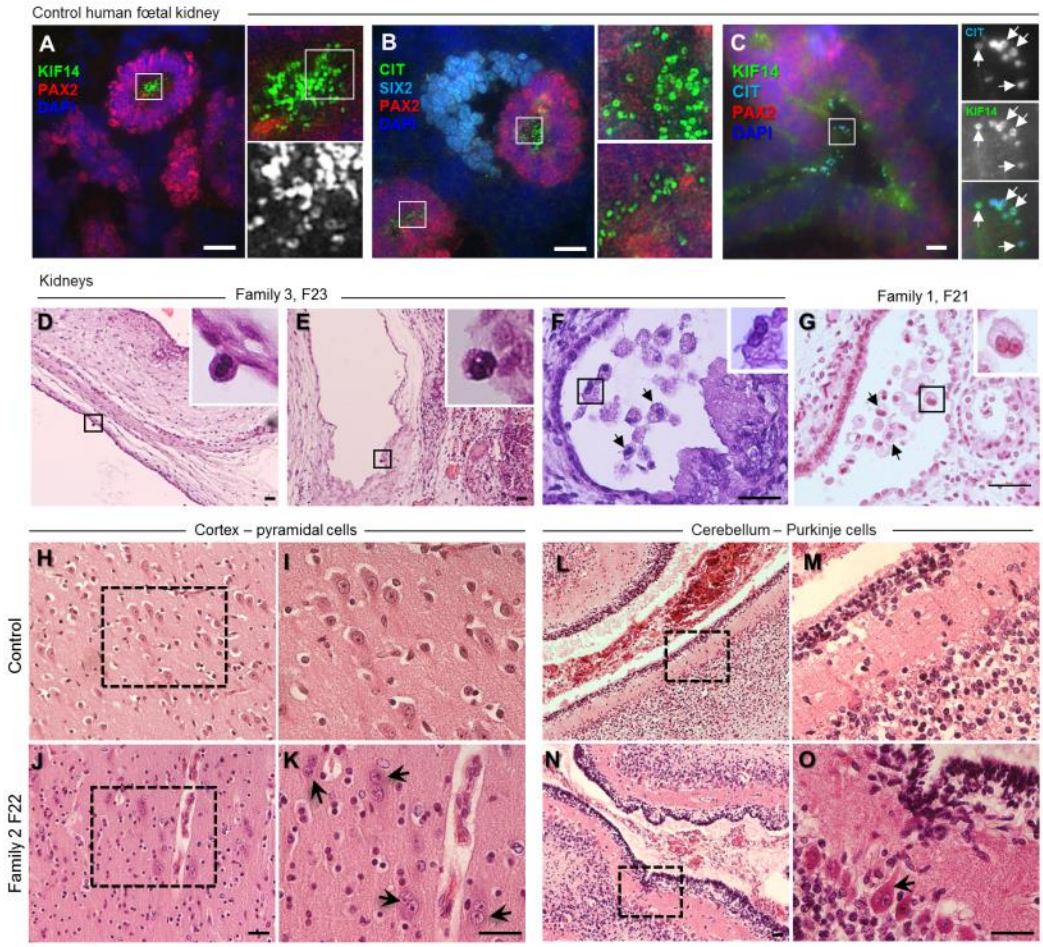

Figure 5. KIF14 is required for cytokinesis in developing human kidney and brain. (A-C) Sections of control human foetal kidneys (23 weeks) were stained for: (A) KIF14 (green), PAX2 (red) and Hoechst (blue), (B) CIT (green), SIX2 (red), PAX2 (cyan), and Hoechst (blue), and (C) KIF14 (green), PAX2 (red), CIT (cyan), and Hoechst (blue). Insets show higher magnification of regions of interest, denoted by the white outline, and arrows point to ring-like structures corresponding to midbodies. Similar results were obtained in 3 other control foetuses. (D-G) Haematoxylin-eosin staining of kidney sections from foetus 23 from family 3 (D-F) and from foetus 21 from family 1 (G) showed the presence of binucleated cells (black boxes) which were enlarged in the corresponding insets. (H-O) Haematoxylin-eosin staining of the brain cortex (H-K) and cerebellum (L-O) from a control foetus (37 weeks) and foetus 22 from family 2, as indicated. Binucleated pyramidal neurons and Purkinje cells are highlighted by black arrows. Scale bars: 10 µm (A-C), 50 µm (D-O).

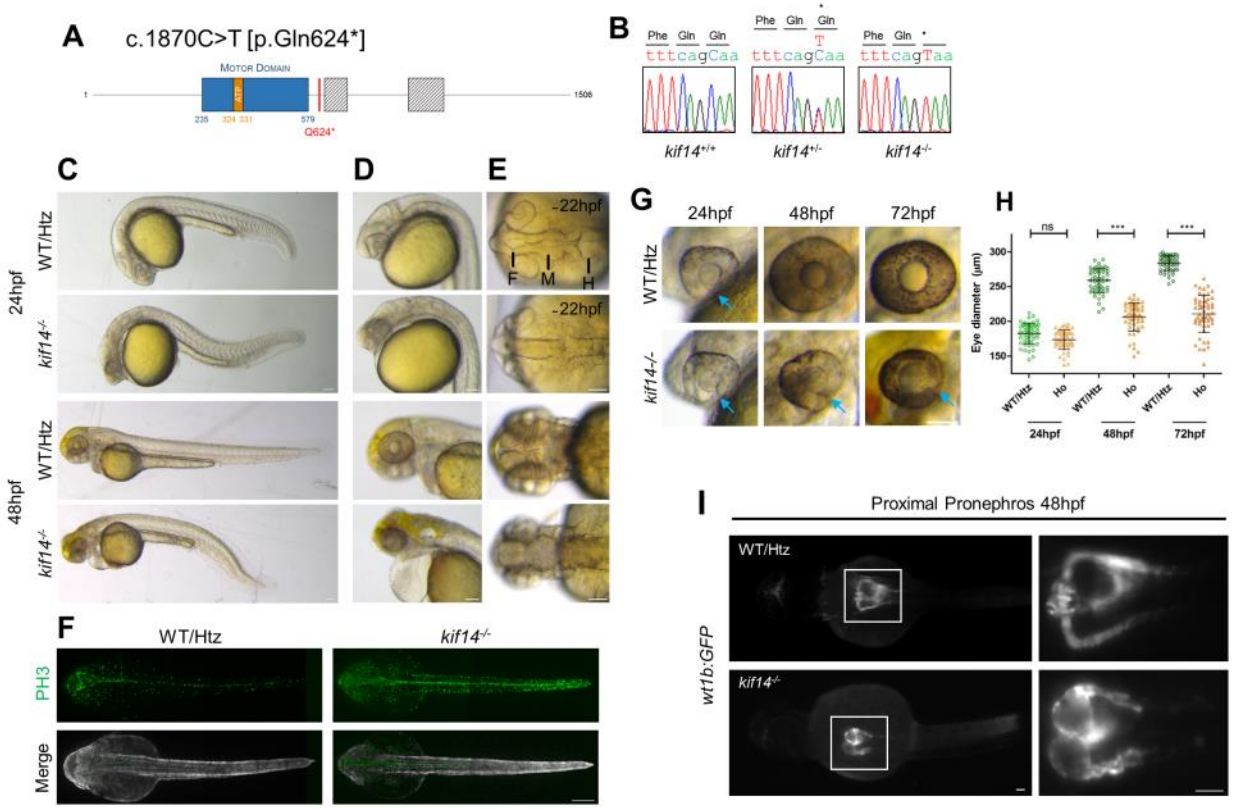

Figure 6. ***In vivo*** **zebrafish model reveals loss of** ***kif14*** **causes severe developmental defects of the brain and kidneys.** (A) Schematic representation of zebrafish *kif14* showing the position of the nonsense mutation. The motor and coiled-coil domains are also shown. (B) DNA trace from Sanger sequencing of exon 11 of *kif14* in WT, heterozygous and homozygous embryos showing the nucleotide, and subsequent amino acid, change. (C-E) Representative images of the phenotypes observed in WT/Htz and *kif14*$^{-/-}$ embryos at 24hpf (top row) and 48hpf (bottom row). Scale bars: 100 µm. (D) Higher magnifications of the head region to better observe morphology of the brain and eyes. (E) Top view of the brain of WT/Htz and *kif14*$^{-/-}$ embryos. F, forebrain; M, midbrain; H, hindbrain. (F) Immunofluorescence of WT/Htz and *kif14*$^{-/-}$ embryos at 24hpf immunostained for Phospho-Histone H3 (PH3, green) and AcTub (grey) shown in dorsal views. Scale bars: 200 µm. (G) Representative images of the eyes of WT/Htz and *kif14*$^{-/-}$ embryos at 24hpf, 48hpf and 72hpf. Asterisks denote observed coloboma. Scale bars: 100 µm. (H) Quantification of eye size (diameter). ns = not significant, ***P< 0.0001 from n=3 independent experiments, t-test. (I) Live imaging of *Tg(wt1b:GFP)* WT/Htz and *kif14*$^{-/-}$ embryos at 48hpf, dorsal view, with anterior to the left. Inset shows a higher magnification of proximal pronephros. Scale bars: 200 µm.

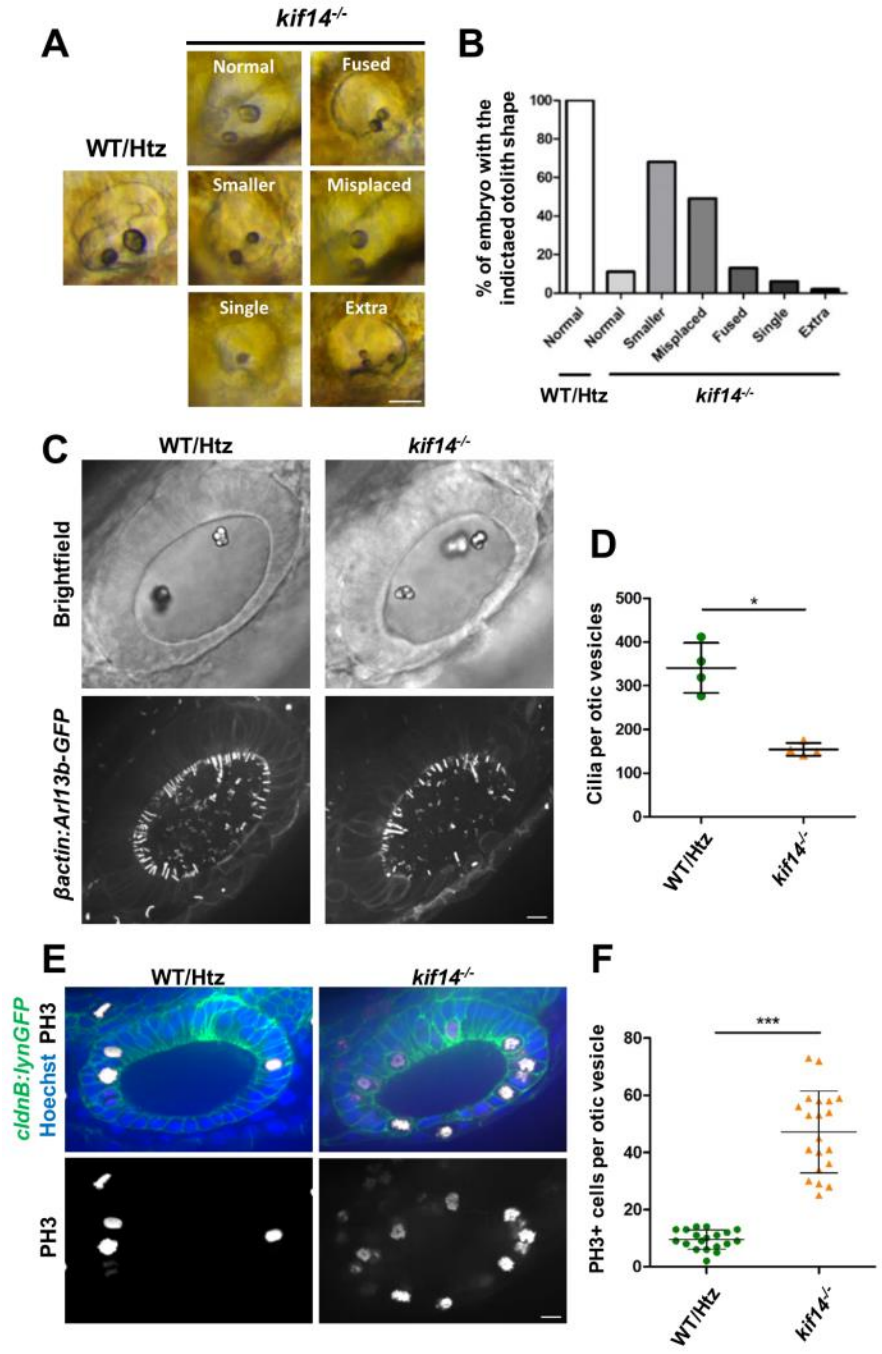

Figure 7. ***In vivo*** **zebrafish model presents ciliopathy-like phenotypes likely due to an accumulation of cells blocked/delayed in mitosis.** (A,B) Representative images (A), and quantification (B; n=61; 3 separate clutches), of otolith phenotypes observed at 72hpf in WT/Htz and *kif14*$^{-/-}$ embryos. (C, D) Live confocal imaging in brightfield (top row) and for GFP (cilia, bottom row) of *Tg(act2b:Arl13b-GFP)* of a representative otic vesicle of WT/Htz and *kif14*$^{-/-}$ embryos at 24hpf (C). Quantification of the number of cilia (Arl13b-GFP) in the otic vesicle (D). (E, F) Immunofluorescence of PH3 (white), and Hoechst (blue) stained *Tg(cldnB:GFP)* otic vesicles at 24hpf (E) and quantification of PH3+ nuclei in the otic vesicle (F). *P< 0.01, ***P< 0.0001 from n=2 independent experiments, t-test (D, F). Scale bars: 10 µm.

Abbreviations:

Renal hypodysplasia (RHD)

Loss-of-function (LOF)

Primary cilia (PC)

Congenital Anomalies of the Kidney and Urinary Tract (CAKUT)

Meckel-Gruber syndrome (MKS)

Ureteric bud (UB)

Malformations of cortical development (MCD)

acetylated α-tubulin (AcTub)

Hours post fertilisation (hpf)

Phospho-histone H3 (PH3)